



## Dynamics of Spiking Neurons Connected by Both Inhibitory and Electrical Coupling

TIMOTHY J. LEWIS AND JOHN RINZEL

*Center for Neural Science and Courant Institute for Mathematical Science, New York University,  
4 Washington Place, Rm 809, NY 10003, USA*

tim.lewis@nyu.edu

*Received March 1, 2002; Revised December 16, 2002; Accepted December 13, 2002*

Action Editor: Carson C. Chow

**Abstract.** We study the dynamics of a pair of intrinsically oscillating leaky integrate-and-fire neurons (identical and noise-free) connected by combinations of electrical and inhibitory coupling. We use the theory of weakly coupled oscillators to examine how synchronization patterns are influenced by cellular properties (intrinsic frequency and the strength of spikes) and coupling parameters (speed of synapses and coupling strengths). We find that, when inhibitory synapses are fast and the electrotonic effect of the suprathreshold portion of the spike is large, increasing the strength of weak electrical coupling promotes synchrony. Conversely, when inhibitory synapses are slow and the electrotonic effect of the suprathreshold portion of the spike is small, increasing the strength of weak electrical coupling promotes antisynchrony (see Fig. 10). Furthermore, our results indicate that, given a fixed total coupling strength, either electrical coupling alone or inhibition alone is better at enhancing neural synchrony than a combination of electrical and inhibitory coupling. We also show that these results extend to moderate coupling strengths.

**Keywords:** synchrony, electrical coupling, gap junctions, inhibition

### 1. Introduction

Synchronous oscillatory activity has been observed in populations of cortical neurons, and it has been suggested that this activity may be important for cognition and sensory information processing. However, the functional significance of synchrony remains a subject of debate (see reviews in *Neuron* vol. 24, 1999). Nevertheless, it behooves us to try to uncover the mechanisms underlying these oscillations. An understanding of how and when synchronous oscillations arise could provide insight into their function.

GABAergic interneurons appear to be critically involved in synchronous population activity that has been observed both *in vivo* and *in vitro* (see McBain and Fisahn, 2001; Ritz and Sejnowski, 1997; Buzsáki and Chrobak, 1995). Although some rhythmic activ-

ity seems to rely on the interaction of inhibitory interneurons and excitatory principle cells (Fisahn et al., 1998; Buhl et al., 1998), synchronized spontaneous activity has also been shown to exist in networks formed exclusively of interneurons (Beierlein et al., 2000; Whittington et al., 1995, 1997). This is consistent with theoretical studies that have demonstrated that, contrary to traditional dogma, inhibitory coupling can act to synchronize the activity of oscillatory neurons under certain conditions, e.g. when synapses are sufficiently slow (van Vreeswijk et al., 1994; Wang and Buzsáki, 1996; Wang and Rinzel, 1992). Modeling work however has demonstrated that mild heterogeneity can sometimes destroy the ability of inhibition to produce synchronized activity (White et al., 1998; Wang and Buzsáki, 1996; Golomb et al., 1994).

Recently investigations have revealed that many local interneuronal networks throughout the brain display electrical coupling through gap junctions (see Galarreta and Hestrin, 2001a). There are different subpopulations of interneurons, and it has been found that the electrical coupling is predominantly between cells of the same subpopulation (Gibson et al., 1999; Beierlein et al., 2000; Amitai et al., 2002). This suggests that interneurons could be organized into functional groups of cells. Traditionally, electrical coupling has been thought to promote synchrony, and indeed electrical coupling seems to induce synchrony in some isolated networks of cortical interneurons (Beierlein et al., 2000; Michelson and Wong, 1994; Benardo, 1997; Traub, 1995; Traub et al., 2001). However, weak electrical coupling can sometimes foster antisynchronous activity as well (Chow and Kopell, 2000; Skinner et al., 1999; Han et al., 1995; Sherman and Rinzel, 1994).

Some interneuronal networks, such as networks of fast-spiking interneurons, are extensively connected by both inhibition and electrical coupling (Galarreta and Hestrin, 1999; Gibson et al., 1999). An exact role for combined electrical and inhibitory coupling is yet to be determined. It has been suggested that the presence of electrical coupling between interneurons could add robustness to inhibition-induced synchrony (White et al., 1998; Traub et al., 2001). Cell-pair recordings have led to the suggestion that inhibition and electrical coupling in interneuronal networks act synergistically to enhance neuronal synchronization of fast-spiking interneurons (Tamás et al., 2000). Furthermore, a modeling study has shown that electrical coupling can stabilize bursting activity in mutually inhibiting cell-pairs (Skinner et al., 1999). However, as mentioned above, electrical coupling can foster antisynchronous activity, and recurrent inhibition leads to antisynchronous activity when synaptic dynamics are sufficiently rapid. Thus, a global picture of how the interaction of these two coupling modes affect the network dynamics remains elusive. It is unclear what circumstances allow synchrony to arise, and what advantages, if any, combined coupling has over either electrical or inhibitory coupling alone.

Here, we study pairs of intrinsically oscillating leaky integrate-and-fire (LIF) cells connected by reciprocal inhibition and electrical coupling. Phase-locking patterns in the cell-pairs are systematically examined over a wide range of intrinsic frequencies and coupling parameters. The ultimate goal of our work is to build a qualitative framework for understanding how combi-

nations of electrical and inhibitory coupling affect dynamics in neuronal networks. We focus on cell-pairs, because in vitro cell-pair recordings (Gibson et al., 1999; Galarreta and Hestrin, 1999; Tamás et al., 2000) provide a direct experimental analog to our model (see Discussion). We can therefore make experimentally testable predictions using the two cell model.

In the section entitled “Leaky integrate-and-fire model for coupled cells” (Section 2), we provide a thorough description of the LIF cell-pair model and describe the basic types of behavior that the model exhibits. In “Weak coupling” (Section 3), we introduce the basic concepts of the theory of weakly coupled oscillators and apply the theory to obtain the phase-locking properties of LIF cell-pairs with weak inhibition alone, weak electrical coupling alone and combinations of two coupling modes. The principle results of the paper are contained within Fig. 10. We show that the results obtained for weak coupling extend to cell-pairs with moderate coupling in “Beyond weak coupling” (Section 4). Finally, in the Discussion (Section 5), we summarize the results of the paper, discuss their implications, and make predictions for in vitro experiments on cell-pairs connected by inhibitory and electrical coupling.

## 2. Leaky Integrate-and-Fire (LIF) Model for Coupled Cells

In this section, we describe the intrinsic dynamics and the coupling terms of an LIF cell-pair model. The model includes only the basic features of spiking neurons and coupling dynamics. The simplicity of the model allows for an extensive analysis of the phase-locking properties of the system. This analysis provides a theoretical framework with which to understand behavior of more complicated models and experimental preparations, as well as the in situ physiological system.

### 2.1. Model Description

Consider two identical cells connected by electrical and inhibitory coupling. The intrinsic dynamics of individual cells are described by single-compartment leaky integrate-and-fire (LIF) neurons:

$$c_m \frac{dV_j}{dt} = -g_m(V_j - V_r) + I_{app}, \quad j = 1, 2. \quad (1)$$

where  $t$  is time,  $c_m$  is the membrane capacitance,  $V_j$  is the transmembrane potential of the  $j$ th cell ( $j = 1, 2$ ),  $V_r$  is the resting potential of the cells (the reversal potential of the leakage current),  $g_m$  is the membrane conductance of each cell, and  $I_{app}$  is a constant current applied to the cells. When  $V_j$  reaches a threshold potential  $V_{th}$ , cell  $j$  “fires a spike” and  $V_j$  is reset to the potential  $V_{reset}$ .

Given the initial condition of  $V_j = V_{reset}$ ,  $V_j$  for isolated cells increases according to the expression

$$V_j(t) = V_{reset} + \frac{I_{app} + g_m(V_r - V_{reset})}{g_m}(1 - e^{-t g_m/c_m}).$$

If  $I_{app} \leq g_m(V_{th} - V_r)$ , then the cell approaches a steady state  $V_j^* = V_r + I_{app}/g_m \leq V_{th}$  and never fires. If  $I_{app} > g_m(V_{th} - V_r)$ , then  $V_j$  increases exponentially from  $V_{reset}$  until  $V_j = V_{th} < V_r + I_{app}/g_m$  at which point the cell fires,  $V_j$  is reset to  $V_{reset}$  and the process is repeated. Thus, the cell undergoes periodic firing at a frequency

$$f = \left[ \frac{c_m}{g_m} \ln \left( \frac{I_{app} - g_m(V_{reset} - V_r)}{I_{app} - g_m(V_{th} - V_r)} \right) \right]^{-1}, \quad (2)$$

i.e. the period is  $T_0 = 1/f$ . This relationship between  $I_{app}$  and  $f$  (or  $T_0$ ) implies that one can always identify increases in the current applied to a cell  $I_{app}$  with increases in the cell’s intrinsic firing rate  $f$ , as we will often do in what follows. An absolute refractory period following spikes should only have significant effects on firing patterns at very high frequencies and therefore is not included in the model.

Coupling terms are included as additional current terms on the right-hand side of Eq. (1).

Chemical synaptic coupling is modeled by alpha-function current injection (in both theoretical work (Neltner et al., 2000; van Vreeswijk et al., 1994) and experimental studies (Oviedo and Reyes, 2002; Stuart and Sakmann, 1995)). Each time cell  $k$  fires, a fixed inhibitory postsynaptic current is injected into cell  $j$ . This current is taken to have the shape of an alpha-function

$$I_{syn,jk}(t) = -q_s S_{jk}(t) = -q_s \alpha^2 t e^{-\alpha t}, \quad t \geq 0, \quad j = 1, 2, \quad j \neq k. \quad (3)$$

The parameter  $\alpha$  is the reciprocal of the synaptic time constant and will be used as a measure of the speed of the synaptic dynamics (units of 1/time). The parameter  $q_s$  is a measure of the synaptic strength (units of charge). The alpha functions are normalized so that the

total charge injected with each inhibitory current input equals  $-q_s$ . During repetitive firing, the inhibitory postsynaptic currents sum linearly. When cell  $k$  fires  $T$ -periodically at times  $t = nT$ , one can find an analytical form for the  $T$ -periodic total synaptic current injected into cell  $j$  by summing the resulting geometric series

$$\begin{aligned} I_{syn,jk}(t) &= - \sum_{n=-\infty}^0 q_s S_{jk}(t - nT), \\ &= -q_s \frac{\alpha^2}{(1 - e^{-\alpha T})^2} e^{-\alpha(t-nT)} \\ &\quad \times [(t - nT)(1 - e^{-\alpha T}) + T e^{-\alpha T}], \\ &= -q_s S_T(t - nT). \end{aligned} \quad (4)$$

for  $t \in [nT, (n+1)T]$ ,  $n = -\infty, 0$ .

The effect of electrical coupling on a cell is described by two terms. The first term is the usual ohmic resistance description. The current flowing from cell  $k$  to cell  $j$  via electrical coupling is  $g_c(V_k - V_j)$ , where  $g_c$  is the electrical coupling conductance (Gibson et al., 1999; Galarreta and Hestrin, 1999; Chow and Kopell, 2000; Usher et al., 1999; Traub, 1995).

The second term in the description of electrical coupling accounts for the effect of the suprathreshold portion of the spike. Integrate-and-fire models usually do not include this portion of spike explicitly, i.e. once the transmembrane potential reaches threshold, it is reset to the more hyperpolarized value  $V_{reset}$ . However, it was recently shown that the electrotonic effect of the suprathreshold portion of spikes can be important in determining phase-locking patterns (Chow and Kopell, 2000), and therefore it must be included in any adequate model of electrically coupled cells. In our model, the effect is accounted for by injecting a delta-function current pulse  $g_c \beta \delta(t)$  into a cell each time a cell coupled to it fires. This instantaneously kicks the membrane potential of the cell towards threshold by a fixed amount,  $g_c \beta$ . The scaling-factor  $\beta$  scales the total charge injected with each delta-function current pulse. We will use  $\beta$  as a measure of the magnitude of the spike effect.

This method of modeling the effect of the suprathreshold portion of the spikes can be justified as follows. Consider two cells, cell  $k$  and cell  $j$ , that are electrically coupled with a coupling strength  $g_c$ . Spikes in a cell generally have a characteristic shape and because membrane conductance is high during a spike, weak to moderate coupling to another cell should have a negligible effect on this characteristic shape of the spikes. Therefore, we can take the

membrane potential of the cells during a spike to be  $V_{spike}(t)$ . It is usually a reasonable assumption that  $V_{spike}(t) \gg V_{th} \geq V_j(t) \geq V_{reset}$  during most of the spike. This implies that if cell  $k$  fires while cell  $j$  is subthreshold, then coupling current flowing from cell  $k$  to cell  $j$  is

$$I_{spike}(t) = g_c [V_{spike}(t) - V_j(t)] \sim g_c [V_{spike}(t)].$$

The total coupling current (i.e. charge) flowing from cell  $k$  to cell  $j$  during the spike is obtained by integrating  $I_{spike}$  over the width of the spike ( $w$ )

$$I_{tot} = \int_0^w I_{spike}(t) dt = g_c \left( \int_0^w V_{spike}(t) dt \right) = g_c \beta.$$

If the spike is sufficiently narrow, then this current is delivered almost instantaneously. Thus, the coupling current during a spike can be approximated by  $g_c \beta \delta(t)$ .

It is useful to nondimensionalize the model equations. We rescale the membrane potential as  $v = (V - V_{reset}) / (V_{th} - V_{reset})$ , so that  $v_{reset} = 0$  and  $v_{th} = 1$ , and we rescale time by the membrane time constant  $c_m / g_m$ ,  $\bar{t} = t / (c_m / g_m)$ . After rescaling, we can collect parameters into groups and name the groups:  $\bar{\alpha} = \alpha c_m / g_m$ ,  $\bar{g}_s = g_s / (c_m (V_{th} - V_{reset}))$ ,  $\bar{g}_c = g_c / g_m$ ,  $\bar{\beta} = \beta / (V_{th} - V_{reset})$ , and  $I = (I_{app} + g_m (V_r - V_{reset})) / (g_m (V_{th} - V_{reset}))$ . Thus, the number of parameters is reduced from nine parameters to five dimensionless parameters. It is important to note that when we examine the dependence of phase-locking patterns on  $I$  and the four coupling parameters ( $\bar{g}_s$ ,  $\bar{\alpha}$ ,  $\bar{g}_c$ ,  $\bar{\beta}$ ), the dependence of all nine dimensional parameters are being studied, although this will not be explicitly stated elsewhere.

For convenience, we drop the bars over the parameters and time, i.e. in what follows,  $t$ ,  $\alpha$ ,  $\beta$ ,  $g_s$ ,  $g_c$  correspond to the dimensionless quantities.

The resulting dimensionless equations describing the two-cell system are

$$\left\{ \begin{array}{l} \frac{dv_1}{dt} = -v_1 + I - g_s \sum_{n=-\infty}^0 s_{12}(t - t_{n,2}) \\ \quad + g_c \left[ (v_2 - v_1) + \beta \sum_{n=-\infty}^0 \delta(t - t_{n,2}) \right] \\ \frac{dv_2}{dt} = -v_2 + I - g_s \sum_{n=-\infty}^0 s_{21}(t - t_{n,1}) \\ \quad + g_c \left[ (v_1 - v_2) + \beta \sum_{n=-\infty}^0 \delta(t - t_{n,1}) \right] \end{array} \right. \quad (5)$$

where  $t_{n,j}$  are the past firing times of the cell  $j$  and  $g_s s_{jk}(t - t_{n,j})$  is the dimensionless inhibitory postsynaptic current injected into cell  $j$  when cell  $k$  fires at time  $t_{n,j}$ , with  $s_{jk}(t) = \alpha^2 t e^{-\alpha t}$ . (Note that  $s_T(t)$  is the dimensionless version of  $S_T(t)$  from Eq. (4)). The parameters  $g_c$  and  $g_s$  are the dimensionless strengths of the electrical and inhibitory connections respectively;  $\alpha$  is a measure of the speed of the synapse,  $\beta$  scales the effect of the suprathreshold portion of the spike and  $I$  is the dimensionless applied current.

## 2.2. Basic Phase-Locking Behavior: Numerical Simulations

The phase-locking properties (or synchronization properties) of this LIF model with either inhibitory or electrical coupling alone follow behavior that has been previously described (van Vreeswijk et al., 1994; Chow and Kopell, 2000). Traditionally, it has been assumed that inhibitory synaptic coupling pushes neurons towards antisynchrony. For sufficiently rapid synaptic dynamics, this is usually the case. Figure 1 (left) shows an example of this in a numerical simulation of the LIF model with  $I = 1.1$ ,  $\alpha = 3$ ,  $g_s = 0.2$  and  $g_c = 0.0$ . However, if the time scale of the synapses is sufficiently slow with respect to the intrinsic oscillation period of the individual cells, inhibition can act to synchronize oscillatory activity (van Vreeswijk et al., 1994; White et al., 1998). This is seen for the LIF model with  $I = 1.6$ ,  $\alpha = 3$ ,  $g_s = 0.2$  and  $g_c = 0.0$  in Fig. 1 (right), i.e. the intrinsic frequency of the cells in Fig. 1 (right) is higher than that in Fig. 1 (left).

Electrical coupling is usually thought to synchronize activity, however it has been shown that electrical coupling can induce stable antisynchronous activity in some cases (Chow and Kopell, 2000; Han et al., 1995; Sherman and Rinzel, 1994). Numerical simulations demonstrate that stable synchronous and antisynchronous states can exist in LIF cell-pairs with weak or moderate electrical coupling as shown in Fig. 2. The simulations suggest that synchrony occurs at high frequency and antisynchrony is more prevalent at low frequencies.

Simulated dynamics for the LIF model with combined electrical and inhibitory coupling show qualitatively similar behavior to that with either type of coupling alone: synchrony at sufficiently high frequency and antisynchrony at sufficiently low frequency.

Our goal is to characterize how synchronization patterns depend on the cells' intrinsic frequency and the

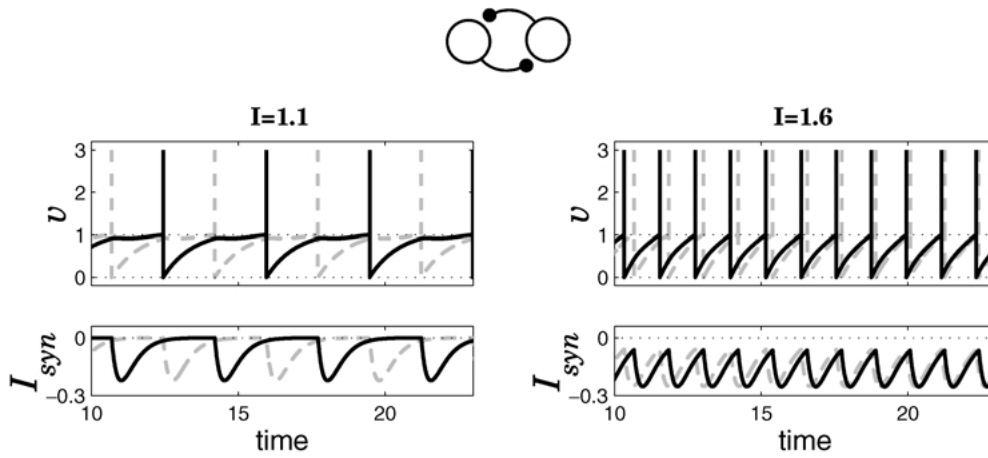


Figure 1. Response patterns of an LIF cell pair coupled by reciprocal inhibition alone: Simulated time courses of transmembrane potential ( $v$ ) and synaptic currents  $I_{syn}$  are shown for the LIF cell-pair model (Eqs. (5)) with “moderate” inhibitory coupling,  $g_s = 0.2$ ,  $\alpha = 3$ . The black and grey curves in the  $v$  vs time plots correspond to the membrane potentials of cell 1 and cell 2,  $v_1$  and  $v_2$ , respectively. The black and grey curves in the  $I_{syn}$  vs time plots correspond to the synaptic currents in cell 2 due to the firing of cell 1,  $I_{syn,21}$ , and the synaptic currents in cell 2 due to the firing of cell 1,  $I_{syn,12}$ , respectively. Initial conditions are  $v_1(0) = 0.4$ ,  $v_2(0) = 0.0$ ,  $I_{syn,12}(0) = 0.0$ ,  $I_{syn,21}(0) = 0.0$ . (left) When  $I = 1.1$ , cells have a relatively low intrinsic frequency and the cells can exhibit stable antisynchronous activity. (right) When  $I = 1.6$ , there is a relatively high intrinsic frequency and the system evolves to a synchronous state.

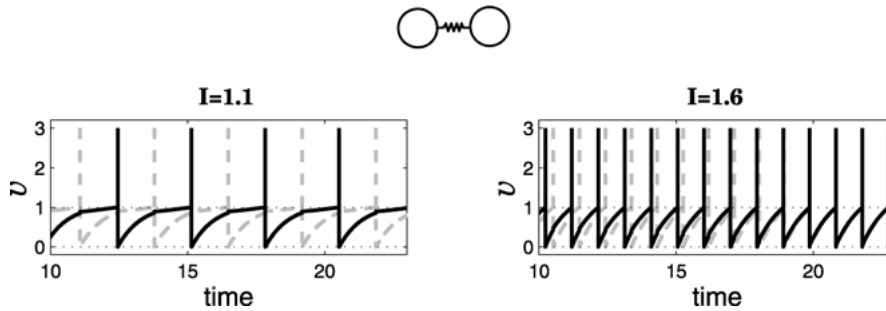


Figure 2. Response patterns of an LIF cell pair coupled by electrical coupling alone: Simulated time courses of transmembrane potential ( $v$ ) are shown for the LIF cell-pair model (Eqs. (5)) with “moderate” electrical coupling,  $\beta = 0.2$ ,  $g_c = 0.2$ . The black and grey curves correspond to the membrane potentials of cell 1 and cell 2,  $v_1$  and  $v_2$ , respectively. Initial conditions are  $v_1(0) = 0.59$ ,  $v_2(0) = 0.0$ . (left) When  $I = 1.1$ , cells fire at a relatively low intrinsic frequency and the cells can exhibit stable antisynchronous activity. (right) When  $I = 1.6$ , there is a relatively high intrinsic frequency and the system evolves to a synchronous state.

coupling parameters, and ultimately how combined electrical and inhibitory coupling influence these patterns. Only a limited amount of information can be obtained using direct numerical simulation of the full LIF model (Eq. (5)). We therefore turn to the theory of weakly coupled oscillators (Kuramoto, 1984).

### 3. Weak Coupling

The theory of weakly coupled oscillators has often been used to analyze networks of neurons coupled by

chemical synapses, e.g. Kopell (1988), Ermentrout and Kopell (1991), Grannan et al. (1993), Hansel et al. (1995), Golomb et al. (2001), and Ermentrout and Kleinfeld (2001). Using this theory enables one to mathematically reduce equations describing a neuronal network to a level that allows extensive analytical insight. The theory shows that, in the limit of weak coupling, the state of each oscillating cell is completely described by its phase in the oscillation, and it yields a system of equations that governs the evolution of the phases in time. This system of equations, known as a phase model, allows one to easily determine the

phase-locked states of the coupled-cell network and the stability of these states.

Although the results from the theory are quantitatively accurate only for sufficiently weak coupling, the qualitative picture generated by the results very often extends to moderate coupling. In Section 4, we will show that this is indeed the case for the LIF model. Moreover, we present our results in a general setting, but our primary intention is to build a framework that is applicable to pairs of cortical interneurons (Gibson et al., 1999), and both electrical and inhibitory coupling between individual cortical interneurons appear to be weak (Gupta et al., 2000; Gibson et al., 1999; Galarreta and Hestrin, 1999). Therefore, interneuron pairs in the cortex lend themselves well to the application of the theory of weakly coupled oscillators and one does not need to push very far to get relevant results.

In Section 3.1, we give a brief, sometimes loose, but hopefully instructive, description of how phase models are obtained using the theory of weakly coupled oscillators. (A similar intuitive description of the theory can be found in Ermentrout and Kleinfeld (2001); for a detailed treatment of the theory, see Kuramoto (1984)). In Sections 3.2–3.6, we apply the theory to coupled LIF cell-pairs, and we show how phase-locking properties of the LIF cell-pairs depend on parameters for three different coupling conditions: inhibition alone, electrical coupling alone, and a combination of these two coupling modes.

Those familiar with the theory of weakly coupled oscillators and phase models may want to skip Section 3.1 and move directly to the subsequent sections.

### 3.1. Reduction to a Phase Model

Consider a pair of weakly coupled cells. Assume that the uncoupled cells intrinsically oscillate with a period  $T$  and that a strongly attracting limit cycle,  $v_{LC}(t)$ ,  $0 \leq t \leq T$ , underlies the oscillations. Because the coupling is weak, the intrinsic dynamics of the cells dominate the dynamics of the coupled-cell system. Each coupled cell strongly adheres to its intrinsic limit cycle  $v_{LC}$  and has a period very close to its intrinsic period  $T$ . The state of each cell is therefore well described solely by its position or “phase” on the limit cycle, where the phase of cell  $j$  is defined as  $[(t/T + \phi_j) \bmod 1]$  with  $0 \leq t \leq T$ ,  $0 \leq \phi_j \leq 1$ . Over each cycle of the oscillations, the weak interactions between the cells can produce small changes in the relative phases of the cells, i.e.  $\phi_j = \phi_j(t)$ . Although these changes are negligible

over a single cycle, these small effects can slowly accumulate and, over many cycles, produce substantial effects on the relative firing times of the cells. Eventually, the coupling interactions can lead to specific timing relationships between the cells such as synchrony (in-phase behavior) or antisynchrony (antiphase behavior). In this subsection, we will derive an equation describing the slow dynamics of the phase difference between coupled cells,  $\phi_j(t) - \phi_k(t)$ .

In order to understand how weak coupling interactions affect the phases of the cells, let us first consider the response of an isolated cell to an abrupt square current pulse. In general, a perturbation of this sort can cause an advance or a delay in the phase of the cell. The magnitude and sign of this “phase shift” depends on the amplitude  $A$  and the duration  $\Delta\tilde{t}$  of the stimulus, as well the time in the cycle at which the stimulus was delivered,  $\tilde{t}$ . The phase resetting curve quantifies this relationship, giving the phase shift  $\Delta\phi$  as a function of  $\tilde{t}$  for a fixed  $A$  and  $\Delta\tilde{t}$ . For sufficiently small and brief stimuli, the phase resetting curve depends linearly on the amplitude and the duration of the stimulus. That is, the phase shift is

$$\Delta\phi = Z(\tilde{t}) A \Delta\tilde{t}, \quad 0 \leq \tilde{t} < T \quad (6)$$

where  $A \Delta\tilde{t}$  is the total charge delivered to the cell by the stimulus and  $Z(\tilde{t})$  describes the proportional phase shift as a function of stimulus timing,  $\tilde{t}$ . The function  $Z(\tilde{t})$  is called the infinitesimal phase resetting curve; it is also aptly known as the phase-dependent sensitivity function.

Now let us return to the weakly coupled cells. As stated above, weak coupling ensures that perturbations due to the coupling are small. This implies that the intrinsic dynamics of the cells dominate, therefore  $v_j(t) \sim v_{LC}(t + \phi_j T)$  and cells fire at times  $(m + \phi_j) T$  with periods that are very close to  $T$ . The relative phases of the cells are time-dependent ( $\phi_j = \phi_j(t)$ ), but they change on a much slower time scale than the period  $T$ .

By simply substituting  $v_{LC}(t + \phi_j T)$  for  $v_j(t)$  into the coupling terms (see Eq. (5)), the amplitude of the coupling current at time  $\tilde{t}$  that cell  $j$  experiences due its connection to cell  $k$  is found to be

$$\begin{aligned} P(\tilde{t} + \phi_j T, \tilde{t} + \phi_k T) &= -g_s s_T(\tilde{t} + \phi_k T) + g_e [(v_{LC}(\tilde{t} + \phi_k T) \\ &\quad - v_{LC}(\tilde{t} + \phi_j T)) + \beta \delta(\tilde{t} + \phi_k T)]. \end{aligned}$$

The presence of this coupling current for a brief time  $\Delta\tilde{t}$  (i.e. from  $\tilde{t}$  and  $\tilde{t} + \Delta\tilde{t}$ ) will lead to a small advance or delay in the timing of cell  $j$ . The magnitude of the phase shift can be approximated simply by multiplying the amplitude of the current, the duration of the current and the sensitivity function  $Z(\tilde{t})$  as in Eq. (6),

$$\Delta\phi_j = Z(\tilde{t} + \phi_j T) P(\tilde{t} + \phi_j T, \tilde{t} + \phi_k T) \Delta\tilde{t}.$$

Dividing the above equation by  $\Delta\tilde{t}$ , and taking the limit  $\Delta\tilde{t} \rightarrow 0$ , we get a differential equation describing the evolution of  $\phi_j$ ,

$$\frac{d\phi_j}{d\tilde{t}} = Z(\tilde{t} + \phi_j T) P(\tilde{t} + \phi_j T, \tilde{t} + \phi_k T).$$

This equation can be reduced further so that the explicit time-dependence is eliminated. Because the changes in  $\phi_j$  are much slower than the time scale of  $T$ , we can average over the full period of oscillation  $T$  holding  $\phi_j$  and  $\phi_k$  fixed and obtain an equation describing the rate of change in  $\phi_j$  on a slow time scale.

$$\begin{aligned} \frac{d\phi_j}{dt} &= \frac{1}{T} \int_0^T Z(\tilde{t} + \phi_j T) P(\tilde{t} + \phi_j T, \tilde{t} + \phi_k T) d\tilde{t} \\ &= \frac{1}{T} \int_0^T Z(\tilde{t}) P(\tilde{t}, \tilde{t} - (\phi_j - \phi_k)T) d\tilde{t} \\ &= H(-(\phi_j - \phi_k)) \end{aligned} \quad (7)$$

i.e. the relative phases  $\phi_j$  and  $\phi_k$  are assumed to be fixed with respect to the integral over  $T$  in  $\tilde{t}$ , but they vary in  $t$ . Note that this reduction is not valid when  $T$  is of the same order of magnitude as the time scale for changes due to the weak coupling interactions, however an alternative reduction can be performed in this case (Ermentrout, 1996).

By subtracting Eq. (7) for cell 2 from that for cell 1, a single differential equation is obtained, which describes the evolution of the phase difference between the two coupled cells,  $\phi = \phi_1 - \phi_2$ .

$$\frac{d\phi}{dt} = H(-\phi) - H(\phi) = G(\phi). \quad (8)$$

The zeros of  $G(\phi)$  are steady states  $\phi^*$  of Eq. (8). When  $G(\phi) > 0$ ,  $\phi$  will increase and when  $G(\phi) < 0$ ,  $\phi$  will decrease. Thus, it is easy to see that  $G'(\phi^*) < 0$  and  $G'(\phi^*) > 0$  imply that the steady state  $\phi^*$  is stable and unstable respectively. Each steady state  $\phi^*$  corresponds to a phase-locked state of the coupled-cell system (Eqs. (5)) that has a phase difference  $\phi^*$ .

Steady states at  $\phi^* = 0$  or  $1$  correspond to a single fully synchronous state, whereas  $\phi^* = 0.5$  corresponds to an antisynchronous state. Other values of  $\phi^*$  correspond to asynchronous but non-antisynchronous states. Stability of the phase-locked states of the coupled cell system is simply given by the stability of corresponding steady state  $\phi^*$  with respect to Eq. (8).

### 3.2. Phase Model for LIF Cell-Pairs

The theory of weakly coupled oscillators can be extended to large networks and weakly heterogeneous cells (Kuramoto, 1984; Neltner et al., 2000; Golomb et al., 2001; Ermentrout and Kleinfeld, 2001), but for the present we will consider only pairs of identical cells. Furthermore, although the theory can be applied to cell models described by any number of variables (e.g. any conductance-based model) with a stable limit cycle oscillation, we will only consider the linear LIF model for which a phase model,  $d\phi/dt = G(\phi)$ , can be obtained analytically. This allows one to easily see how phase-locking depends on intrinsic frequency and coupling parameters and can help to develop general principles along these lines.

The phase-dependent sensitivity function  $Z(t)$  for the LIF model (Hansel et al., 1995; Neltner et al., 2000; Golomb et al., 2001) is

$$Z(t) = \begin{cases} \frac{e^t}{IT}, & 0 < t < T \\ 0, & t = 0, T \end{cases}$$

A derivation of  $Z(t)$  for  $0 < t < T$  is presented in the appendix. During the spike-and-reset phase at  $t = 0, T$ ,  $Z(t)$  is taken to be 0. This assumes that during the spike, the cell is not affected by external perturbations (e.g. due to coupling). This is a reasonable assumption, because the input conductance is extremely high during spikes, rendering the cell insensitive to external perturbations. If one includes an absolute refractory period after spikes in the LIF model, then the region over which  $Z(t) = 0$  would extend throughout the spike and the refractory period. Short refractory periods have very little effect on qualitative phase-locking dynamics in the LIF model, and therefore we have chosen to collapse the absolute refractory period to zero duration.

Outside the spike (and refractory period),  $Z(t)$  for the LIF model is strictly positive, and therefore positive currents will always phase advance the cell. This is a characteristic of many neuronal oscillators, especially

at low firing rates, and is sometimes referred to as type I phase resetting (Hansel et al., 1995; Ermentrout, 1996). The LIF phase resetting curve is an increasing function and it is concave up. This implies that, as  $v$  increases towards threshold, the cell is increasingly sensitive to perturbations and the rate of this increasing sensitivity is itself increasing.

In dimensionless form, the periodic oscillations of the individual LIF cells are given by  $v_{LC}(t) = I(1 - e^{-t})$ ,  $0 < t < T$ . By plugging the expressions for  $Z(t)$ ,  $v_{LC}(t)$ ,  $I_{syn}(t)$  and the spike effect (see Section 2.1) into the equations described in the previous subsection and integrating, we get the  $G$ -function,  $G(\phi)$ , for the LIF model. In the remainder of this section, we evaluate the  $G$ -functions for mutual inhibition alone, for electrical coupling alone and for combined coupling. We then analyze them to show how phase-locked states depend on parameters.

### 3.3. Mutual Inhibition

Using the above expression for  $Z(t)$  and the dimensionless version of the expression for  $I_{syn}$  (Eq. (4)), we can obtain the  $G$ -function for a pair of LIF cells connected by reciprocal inhibition:

$$\begin{aligned}
 G_s(\phi) &= \frac{1}{T} \int_0^T Z(t) [s_T(t - \phi T) - s_T(t + \phi T)] dt \\
 &= \frac{-g_s A}{IT^2(1 - \alpha)^2} \left\{ (e^{-\alpha T} [(T + B)(1 - \alpha) - 1] \right. \\
 &\quad - [B(1 - \alpha) - 1])(e^{\phi T} - e^{(1-\phi)T}) \\
 &\quad + (1 - e^{-T})(e^{\phi T} e^{(1-\alpha)(1-\phi)T} \\
 &\quad \times [(1 - \phi)T + B)(1 - \alpha) - 1] \\
 &\quad \left. - e^{(1-\phi)T} e^{(1-\alpha)\phi T} [(\phi T + B)(1 - \alpha) - 1] \right\}, \tag{9}
 \end{aligned}$$

where  $A = \alpha^2/(1 - e^{-\alpha T})$ ,  $B = T e^{-\alpha T}/(1 - e^{-\alpha T})$  and  $T = \ln(I/(I - 1))$ . Note that the coupling strength  $g_s$  simply scales  $G_s(\phi)$ , therefore it does not effect steady states or their stability. It does however affect the rate at which the system converges to or diverges from the steady states.

Figure 3 shows examples of  $G_s(\phi)$  for three different values of the applied current  $I$ . Note that the  $G$ -functions are symmetric around  $\phi = 0.5$ . This holds for all  $G$ -functions considered here. The symmetry arises because the cells are identical.

For  $I = 1.2$  (Fig. 3 top), the stable steady state at  $\phi^* = 0.5$  corresponds to a stable antisynchronous state,

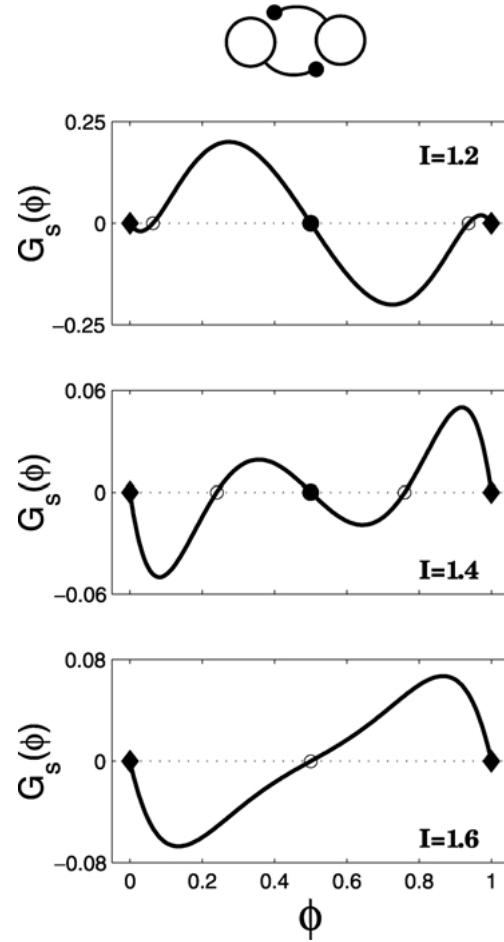


Figure 3.  $G$ -functions ( $G_s(\phi)$ ) for LIF cell-pair connected by weak inhibition alone ( $\alpha = 4.0$ ):  $G_s(\phi)$  determines the phase-locked states of the system in the weak coupling limit (Eq. (8)).  $\phi$  is the phase difference between the cells. When  $G_s(\phi) > 0$ ,  $\phi$  increases; when  $G_s(\phi) < 0$ ,  $\phi$  decreases. The zeros of  $G_s(\phi)$  at  $\phi = \phi^*$  are steady states of Eq. (8) and correspond to phase-locked states with phase difference  $\phi^*$ . If  $G'_s(\phi^*) < 0$ , then the corresponding phase-locked state is stable. If  $G'_s(\phi^*) > 0$ , then the phase-locked state is unstable. Examples of  $G_s(\phi)$  for three different values of  $I$  are shown: (top)  $I = 1.2$ ; (middle)  $I = 1.4$ ; (bottom)  $I = 1.6$ . Stable synchronous states are indicated by filled diamonds. Stable antisynchronous states are indicated by filled circles, whereas unstable antisynchronous and asynchronous states are indicated by open circles.

and the stable steady states at  $\phi^* = 0$  and  $\phi^* = 1$  correspond to a stable synchronous state. There are also unstable steady states at  $\phi^* = 0.05$  and  $\phi^* = 0.95$ . Thus, the system is “bistable”, having both stable synchronous and stable antisynchronous states for the same values of  $I$  and  $\alpha$ . However, although the synchronous state is stable, there is only a 10% chance that it will be realized given a random initial phase

difference  $\phi(0)$ . Note that the unstable steady states act as separatrices, i.e. points separating the basins of attraction of the synchronous and the asynchronous states. With this in mind, it is easy to see that almost all initial phase differences (90%) will converge to the asynchronous state. Thus, asynchrony is the dominant state, which concurs with the traditional view that recurrent inhibition tends to desynchronize activity in cells.

When  $I$  is increased to 1.4 (Fig. 3 middle), all steady states maintain the same stability, but the unstable steady states are closer to  $\phi = 0.5$ , creating a more balanced bistability. The basins of attraction of each state are of comparable sizes. Given a random initial phase difference between the cells, there is about a 50% chance of achieving synchrony and a 50% chance of achieving asynchrony.

When  $I$  is further increased to 1.6 (Fig. 3 bottom), the  $G$ -function is qualitatively different from the previ-

ous two examples. Only the synchronous and asynchronous states exist. Furthermore, the synchronous state ( $\phi^* = 0$  and 1) is stable, but the asynchronous state ( $\phi^* = 0.5$ ) is unstable. Thus, given any initial phase differences between the mutually inhibiting cells, the system always approaches a synchronous state.

An efficient way of showing how phase-locked states depend on parameters over a range of values is by using a bifurcation diagram. The bifurcation diagrams that are included here plot the phase difference of the steady states  $\phi^*$  in relation to the applied current  $I$  (and intrinsic frequency). They show how the values of  $\phi^*$  vary with changes in  $I$ ; they also show the stability of the steady states and the critical values at which there are qualitative changes in behavior, i.e. bifurcation points. Figure 4 shows the bifurcation diagram for the case of pure inhibitory coupling. At sufficiently small  $I$ , the system behaves as shown in Fig. 3 (top) for

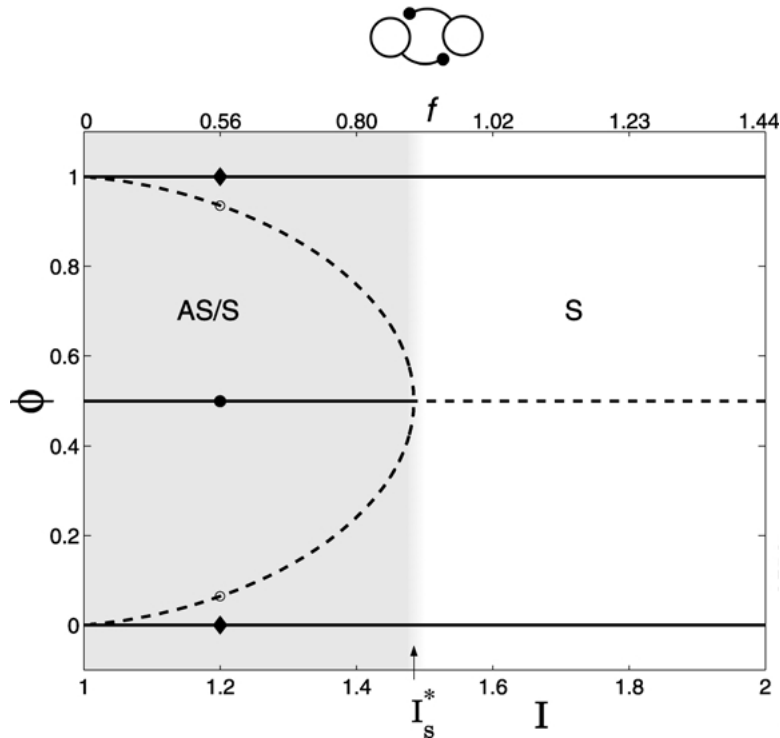
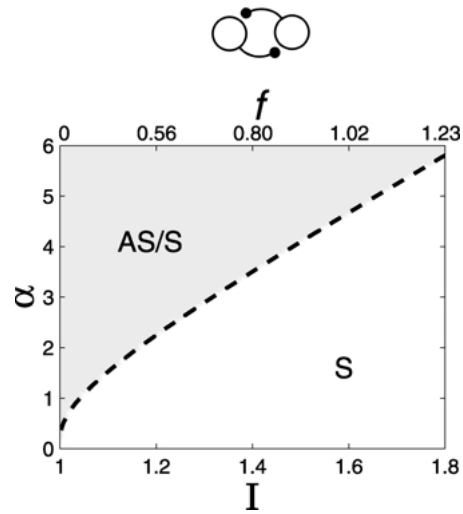


Figure 4. Bifurcation diagram for LIF cell-pair weakly coupled with inhibition alone: phase differences of phase-locked states  $\phi^*$  vs applied current  $I$  or equivalently  $\phi^*$  vs intrinsic frequency  $f$  (see Eq. (2)).  $\alpha = 4.0$ . Solid and dashed lines indicate stable and unstable states respectively.  $I_s^*$  indicates the critical value of  $I$  at which the asynchronous state  $\phi^* = 0.5$  changes stability. For  $I > I_s^*$ , only synchronous activity is stable (white S region), whereas for  $I < I_s^*$ , both synchronous and asynchronous states are stable (grey AS/S region). The filled diamonds, filled circles and open circles indicate the stable synchronous state, stable asynchronous state and the unstable asynchronous states respectively for  $I = 1.2$  (Fig. 3 (top)).

$I = 1.2$  with bistability between the synchronous state,  $\phi^* = 0, 1$ , and the antisynchronous state,  $\phi^* = 0.5$ . For small values of  $I$ , the unstable steady states that define the boundaries of the domain of attraction of  $\phi^* = 0.5$  lie close to  $\phi^* = 0$  and  $\phi^* = 1$ . Therefore, the domain of attraction of  $\phi^* = 0.5$  is large and the antisynchronous state dominates. As  $I$  increases, the domain of attraction of the antisynchronous state shrinks and the antisynchronous state loses its dominance. As  $I$  increases further, the synchronous state becomes dominant, and eventually a critical value  $I_s^*$  is reached where the unstable steady states coalesce with the antisynchronous state. Above this point, the previously unstable steady states do not exist and  $\phi^* = 0.5$  is unstable. This transition is referred to as a subcritical pitchfork bifurcation. A qualitative change in behavior occurs at the critical value  $I_s^*$ : for  $1 < I < I_s^*$ , both the synchronous and antisynchronous states are stable (the AS/S region); for  $I > I_s^*$ , only the synchronous state is stable (the S region).

The bifurcation structure described above is similar to that presented in van Vreeswijk et al. (1994), where bifurcation diagrams for  $\phi^*$  vs  $\alpha$  were plotted for fixed  $I$ . Only the synchronous state is stable for sufficiently small  $\alpha$  (slow synaptic kinetics), whereas both the synchronous and the antisynchronous states are stable when  $\alpha$  is above a critical value. In the  $\phi^*$  vs  $I$  bifurcation diagram, the influence of  $\alpha$  is manifested in the dependence of  $I_s^*$  on  $\alpha$ . We can obtain the relationship between  $I_s^*$  and  $\alpha$  using the equation  $G'_s(\phi^* = 0.5) = 0$ , which is a necessary condition for a change in stability of the steady state  $\phi^* = 0.5$ . This relationship is shown in Fig. 5, where the location of the pitchfork bifurcation is plotted in  $\alpha, I$ -parameter space as a heavy dashed curve. The curve separates  $\alpha, I$ -parameter space into a region where only synchrony is stable and a region where stable synchrony and antisynchrony co-exist. As  $\alpha$  increases,  $I_s^*$  increases, implying that when inhibitory synapses are fast relative to the cells' intrinsic frequency, antisynchronous behavior is promoted, but when synapses are slower relative to the cells' intrinsic frequency, synchrony is promoted.

Note that the zeros of  $G(\phi)$  for excitatory synaptic connections ( $g_s < 0$ ) are the same as those described above for the inhibitory coupling case ( $g_s > 0$ ), however the slopes at these zeros are opposite to one another. Therefore, the phase-locking structure for cells connected by reciprocal excitatory synapses is identical to that described here except that the stability is reversed. This situation for LIF cells coupled by exci-



*Figure 5.* Two parameter response diagram for LIF cell-pair coupled with weak inhibition alone,  $I, \alpha$ -parameter space: The dashed line plots the location of the critical point  $I_s^*$  in relation to  $\alpha$ . (At  $\alpha = 4$ ,  $I_s^* = 1.48$  as in Fig. 4). Above the curve, the synapses are fast relative to the intrinsic frequency and both the synchronous and antisynchronous states are stable (AS/S region, grey); Below the curve, the synapses are slow relative to the intrinsic frequency and only the synchronous state is stable (S region, white). As the speed of the synapses ( $\alpha$ ) increases,  $I_s^*$  increases, i.e. the antisynchronous state is stable over a broader range of  $I$  for faster synapses.

tatory synapses was described by Hansel et al. (1995) and van Vreeswijk et al. (1994).

### 3.4. Electrical Coupling

The  $G$ -function for electrical coupling alone is obtained using the phase-dependent sensitivity function  $Z(t)$  and the coupling current due to the electrical connection between the cells (see Eq. (4)).

$$\begin{aligned}
 G_c(\phi) &= \frac{1}{T} \int_0^T Z(t) g_c [(v_{LC}(t - \phi T) - v_{LC}(t + \phi T)) \\
 &\quad + \beta \delta(t - \phi T) - \beta \delta(t + \phi T)] dt \\
 &= \begin{cases} g_c \frac{2}{T} (\phi \sinh((1 - \phi)T) - (1 - \phi) \\
 \quad \times \sinh(\phi T)) + g_c \frac{\beta}{IT^2} (e^{\phi T} - e^{(1-\phi)T}), \\
 \quad 0 < \phi < 1, \\
 0, \quad \phi = 0, 1. \end{cases}
 \end{aligned} \tag{10}$$

Note that the coupling strength  $g_c$  simply scales the  $G$ -function. It does not affect the existence and stability

of the phase-locked states; it only affects how fast the system approaches or moves away from a phase-locked state.

The term in  $G_c(\phi)$  that is scaled by  $\beta$  accounts for the effect of the suprathreshold portion of the spike. This term, which is shown in Fig. 6(top), always tends to synchronize the cells, i.e. it has a stabilizing effect on  $\phi^* = 0, 1$  and a destabilizing effect on  $\phi^* = 0.5$ .

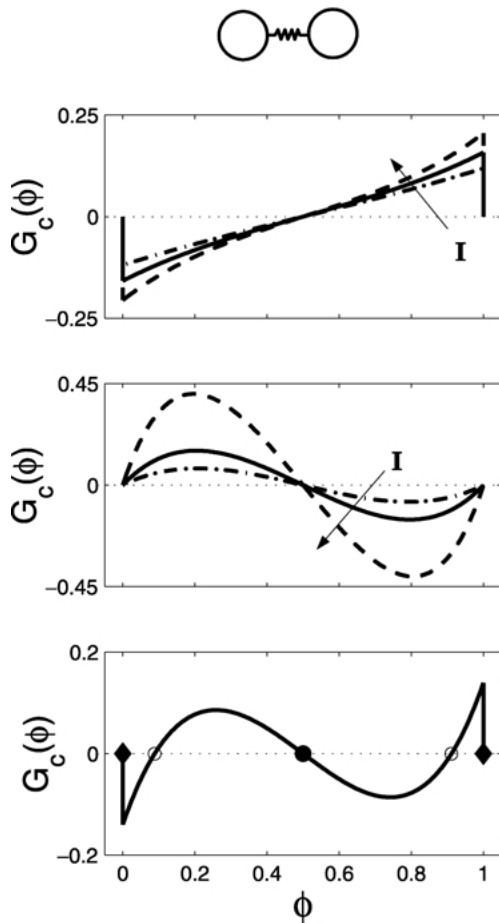


*Figure 6.*  $G$ -functions ( $G_c(\phi)$ ) for LIF cell-pair coupled with weak electrical coupling only: For all panels, dashed lines, solid lines and dot-dashed lines correspond to  $I = 1.05$ ,  $I = 1.15$ , and  $I = 1.3$  respectively.  $G_c(\phi)$  can be dissected into two parts as in Eq. (10). (top) The portion of  $G_c(\phi)$  accounting for the effect of the suprathreshold portion of the spike with  $\beta = 0.1$ . This portion of the  $G$ -function always tends to synchronize activity. (middle) The portion of  $G_c(\phi)$  accounting for the subthreshold activity (obtained by setting  $\beta = 0$ ). This portion of the  $G$ -function always tends to desynchronize activity. (bottom) The full  $G$ -function shown for  $\beta = 0.1$  and  $I = 1.15$ . The filled diamonds, filled circles and open circles indicate the stable synchronous state, stable antisynchronous state and the unstable asynchronous states respectively.

The discontinuity at  $\phi = 0, 1$  is a result of the discontinuity in  $Z(t)$  and the delta-function description of the spike.

Setting  $\beta = 0$  gives the  $G$ -functions for the case when the effect of the suprathreshold portion of the spike is omitted.  $G$ -functions with  $\beta = 0$  are plotted in Fig. 6 (middle). Counter-intuitively, the synchronous state  $\phi^* = 0, 1$  is unstable and the antisynchronous state  $\phi^* = 0.5$  is stable for all  $I$  in this case. This can be understood in terms of the effect of the fast reset (repolarization) of the cells and the shape of their phase-dependent sensitivity function  $Z(t)$ . Consider two coupled cells with a small phase difference. During the slow depolarization towards threshold, the membrane potential in the lagging cell is slightly less than that in the leading cell. Consequently, there is a small positive (depolarizing) current in the lagging cell that flows from the leading cell due to the electrical coupling. This current speeds up the lagging cell and slows down the leading cell, acting to synchronize the cells. However, because the voltage differences are small, the electrotonic current is small and the synchronizing effect is small. Once the leading cell reaches threshold, it is immediately reset and the electrical coupling current switches direction. Now coupling acts to retard the progress to threshold in the lagging cell and to speed up the leading cell. Because the potential difference between the cells is large and the sensitivity of the cells is highest around threshold, the lagging cell is substantially delayed before it fires. This effect is so strong that it overcomes the previous advancing effect and causes the net effect of coupling over an entire period to be desynchronizing.

The full  $G$ -function for  $I = 1.15$  and  $\beta = 0.1$  is a linear combination of the two corresponding curves in Fig. 6 (top) and (middle), and it is shown in Fig. 6 (bottom). Both the synchronous and the antisynchronous states are stable in this case, but if  $I$  is increased above  $I = 1.5$ , only the synchronous state is stable.

The bifurcation diagram  $\phi^*$  vs  $I$  for pure electrical coupling with  $\beta = 0.1$  is plotted in Fig. 7. Surprisingly, it is qualitatively the same as that for inhibitory coupling (Fig. 4). At high  $I$ , the only stable state is the synchronous state, and at sufficiently low  $I$ , stable synchronous and antisynchronous states coexist. The antisynchronous state loses its stability via a subcritical pitchfork bifurcation at the critical value  $I_c^*$ , which depends upon  $\beta$ . By considering  $G'_c(\phi^* = 0.5) = 0$ , one can obtain the relationship between  $I_c^*$  and  $\beta$

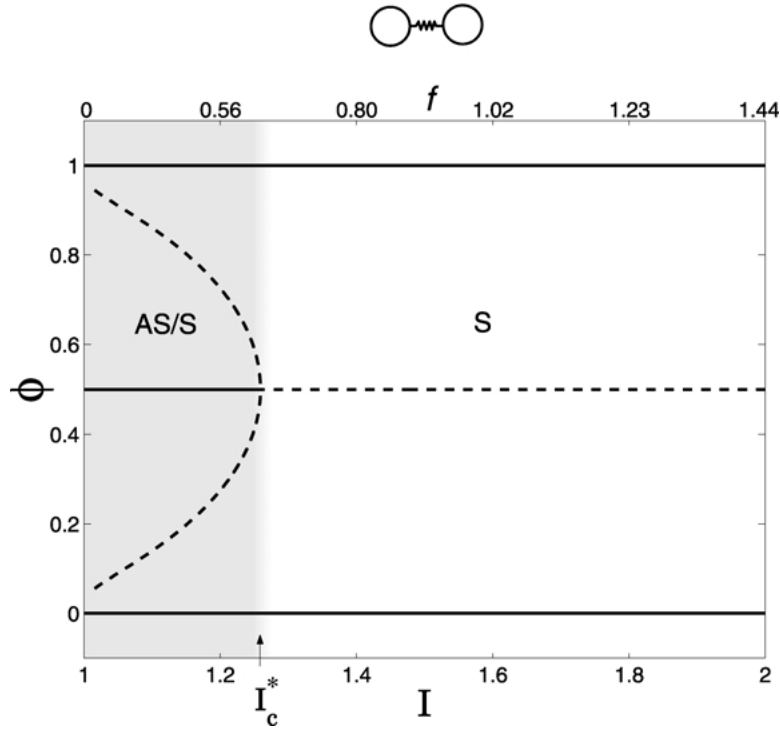


*Figure 7.* Bifurcation diagram for LIF cell-pair with weak electrical coupling alone:  $\beta = 0.1$ . Solid and dashed lines indicate stable and unstable phase-locked states respectively.  $I_c^*$  indicates the critical value of  $I$  at which the antisynchronous state  $\phi^* = 0.5$  changes stability. For  $I > I_c^*$ , only synchronous activity is stable (white S region), whereas for  $I < I_c^*$ , both synchronous and antisynchronous states are stable (grey AS/S region). Note that the bifurcation diagram for electrical coupling alone is qualitatively similar to that for inhibition alone (Fig. 4).

analytically

$$\beta = \left( I_c^* - \frac{1}{2} \right) \ln \left( \frac{I_c^*}{I_c^* - 1} \right) - 1. \quad (11)$$

$I_c^*$  increases as  $\beta$  decreases, as is seen in Fig. 8 (dashed line). This implies that, when the electrotonic effect of the suprathreshold portion of spikes is weak, antisynchrony persists for a larger range of intrinsic frequencies. As the effect vanishes  $\beta \rightarrow 0$ , the critical current at which the antisynchronous state loses stability  $I_c^*$  goes to infinity and the unstable steady states approach the synchronous state. This effectively leaves only the antisynchronous state for all  $I$  (as mentioned above for  $\beta = 0$ ).

The bifurcation structure described in this subsection is equivalent to that described in Chow and Kopell (2000) except in their limit of very high frequency. Because we take the spike to be infinitely thin and Chow and Kopell do not, our LIF model does not include the bifurcations at ultra-high intrinsic frequencies, where the period is approximately twice the width

of the spikes, as seen by Chow and Kopell. This issue is addressed further in the discussion.

### 3.5. Combined Electrical and Inhibitory Coupling

The electrical and inhibitory coupling currents in the LIF model are two distinct terms in the model's Eqs. (5). Thus, the  $G$ -function for combined inhibition and electrical coupling is simply the linear sum of the two individual  $G$ -functions

$$\begin{aligned} G_{sc}(\phi) &= \frac{1}{T} \int_0^T Z(t) [g_s [s_T(t - \phi T) - s_T(t + \phi T)] \\ &\quad + g_c [(v_{LC}(t - \phi T) - v_{LC}(t + \phi T)) \\ &\quad + \beta \delta(t - \phi T) - \beta \delta(t + \phi T)]] dt \\ &= G_s(\phi) + G_c(\phi). \end{aligned} \quad (12)$$

In the cases of either electrical coupling or inhibition alone, the coupling strengths  $g_c$  and  $g_s$  do not play a role in determining the phase-locked states or the stability

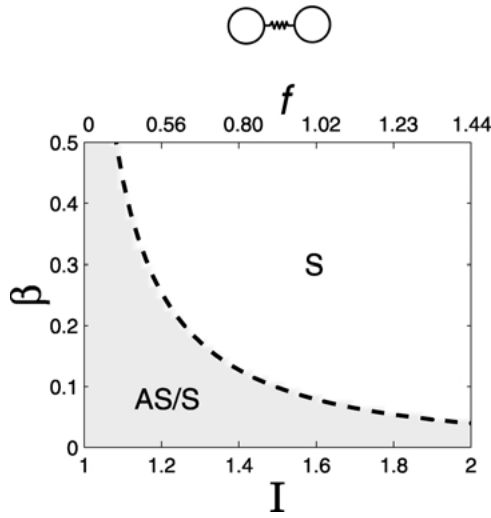


Figure 8. Two parameter response diagram for LIF cell-pair connected by weak electrical coupling alone,  $I$ ,  $\beta$ -parameter space: The dashed curve plots the critical value  $I_c^*$  in relation to  $\beta$  (as in Eq. (11)). For  $(I, \beta)$  values below the curve (AS/S region, grey), cells can exhibit either stable synchrony or antisynchrony. For  $(I, \beta)$  values above the curve (S region, white), cells can only exhibit stable synchrony. As  $\beta$  increases,  $I_c^*$  decreases. This implies that stronger effects of the suprathreshold portion of the spike promotes synchrony.

of these states. In the case of combined coupling, if the coupling strengths are changed such that their ratio remains fixed, then  $G_{sc}(\phi)$  is only changed by a scalar factor, and the phase-locked states and their stability do not change. However, substantial effects can occur when the relative coupling strengths. To study these effects, we introduce the parameter  $\rho$ , which we define to be the fraction of coupling due to electrical coupling,  $\rho = g_c/(g_c + g_s)$ .  $\rho = 1$  corresponds to the case of electrical coupling alone and  $\rho = 0$  corresponds to inhibition alone.

The fact that the total  $G$ -function,  $G_{sc}(\phi)$ , is a linear combination of the individual  $G$ -functions implies a lot about the effects of combined electrical and inhibitory coupling.

Because  $\phi^* = 0, 1$  and  $\phi^* = 0.5$  are zeros of both individual  $G$ -functions, they are also zeros of the combined  $G$ -function, and thus the synchronous and antisynchronous states always exist for combined coupling. The stability of these steady states are given by  $G'_{sc}(\phi^*) = G'_s(\phi^*) + G'_c(\phi^*)$ . Therefore, given fixed values of  $I$ ,  $\alpha$ , and  $\beta$ , if the steady state  $\phi^*$  is stable for both electrical coupling alone and inhibitory coupling alone, then  $\phi^*$  must also be stable for all combinations of electrical and inhibitory coupling ( $0 < \rho < 1$ ), i.e.

$G'_c(\phi^*) < 0$  and  $G'_s(\phi^*) < 0$  imply that  $G'_{sc}(\phi^*) < 0$ . A similar argument holds for instability. This implies that the synchronous state  $\phi^* = 0, 1$  is always stable for any combination of electrical and inhibitory coupling as in the cases of the single coupling modes. It also implies that, for any combination of coupling, the anti-synchronous state  $\phi^* = 0.5$  is unstable for sufficiently large  $I$  and stable for sufficiently small  $I$ . Furthermore, it can be shown that for fixed values of  $\alpha$  and  $\beta$  and any combination of coupling ( $0 < \rho < 1$ ),  $I_{sc}^*$ , the critical value of  $I$  at which the antisynchronous state changes stability, must lie between  $I_c^*$  and  $I_s^*$ , the critical values for the cases of the single coupling modes. These characteristics are seen in the bifurcation diagram in Fig. 9 with  $\rho = 0.5$ .

In Fig. 9, the unstable intermediate steady states ( $\phi^* \neq 0, 1$  or  $0.5$ ) for combined coupling fall between the unstable intermediate steady states for cases of the single coupling modes. It can be shown that this property necessarily holds for all  $0 < \rho < 1$ . It is possible that the system with combined coupling could have more than one intermediate steady state between the intermediate steady states of the the single coupling cases for a fixed values of  $\alpha$ ,  $\beta$  and  $\rho$ . If indeed more than one intermediate steady state exists, then there would be an odd number of these states, some of which would be stable. However, we have never observed this.

Various properties arising from the combination of electrical and inhibitory coupling can be seen from inspecting Fig. 10. Indeed, Fig. 10 summarize the principle results of this paper.

Recall that  $I_c^*$  depends on the speed of the synapse  $\alpha$  and that  $I_s^*$  depends on the effect of the suprathreshold portion of the spike  $\beta$ . When the spike effect is relatively small and inhibition is relatively slow,  $I_c^* > I_s^*$ . When the spike effect is relatively large and inhibition is relatively fast,  $I_c^* < I_s^*$ . As stated above,  $I_{sc}^*$  must fall in between  $I_c^*$  and  $I_s^*$  for all  $\rho$ . By further consideration of  $G'_{sc}(\phi^* = 0.5) = 0$ , it can also be proven that  $I_{sc}^*$  either monotonically increases or monotonically decreases with  $\rho$ . These monotonic relationships are shown for the two cases by the heavy dashed lines in Fig. 10.

The grey-scale in Fig. 10 indicates the level of dominance of the synchronous state. Specifically, it shows the probability that the cells will evolve to the synchronous state given a random initial phase difference between the cells. This probability is determined by the phase differences of the unstable intermediate steady states as previously described. For  $I > I_{sc}^*$ , all initial

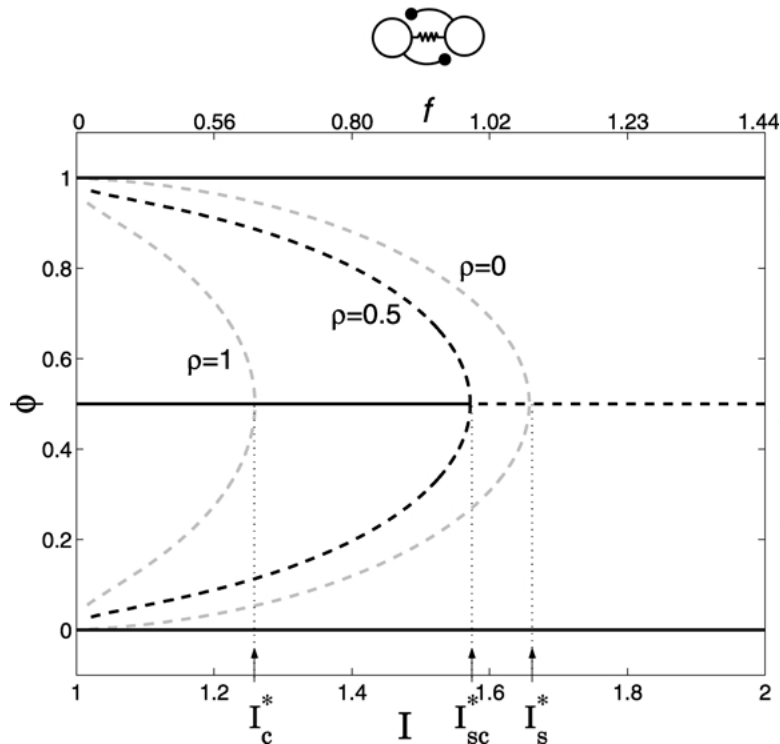


Figure 9. Bifurcation diagram for LIF cell-pair with combined weak electrical coupling and weak inhibition:  $\alpha = 5.0$ ,  $\beta = 0.2$  and  $\rho = 0.5$ , where  $\rho$  is the fraction of electrical coupling,  $g_c/(g_c + g_i)$ . Dark solid and dark dashed lines indicate stable and unstable states respectively.  $I_{sc}^*$  indicates the critical value of  $I$  at which the antisynchronous state  $\phi^* = 0.5$  changes stability. Also, portions of the bifurcation diagrams for electrical coupling alone ( $\rho = 1.0$ ,  $\beta = 0.2$ ) and inhibitory coupling alone ( $\rho = 0.0$ ,  $\alpha = 5.0$ ) are shown as light curves;  $I_s^*$  and  $I_c^*$  are indicated as well.  $I_{sc}^*$  must always lie between  $I_s^*$  and  $I_c^*$ , however the ordering of  $I_s^*$  and  $I_c^*$  can be reversed.

phase differences will lead to the synchronous state. Below  $I_{sc}^*$ , the antisynchronous state becomes increasingly dominant as  $I$  decreases with  $\rho$  fixed. This is also seen in Fig. 9 for  $\rho = 0.5$ . Changing  $\rho$ , the fraction of the total coupling due to electrical coupling, with  $I$  fixed can have different effects in different situations. Figure 10 (left) shows a case where inhibitory kinetics are relatively fast and spike effect is large so that  $I_c^* < I_s^*$ . In this case, if  $I_c^* < I < I_s^*$ , then the dominance of the antisynchronous state decreases as  $\rho$  increases ( $g_c$  increases and/or  $g_s$  decreases) and the cells pair can switch from an antisynchronous state to a synchronous state by increasing  $\rho$ . This implies that adding electrical coupling to an inhibitory network would promote synchrony. Alternatively, Fig. 10 (right) shows a case for which the spike effect is relatively small and inhibitory kinetics are relatively slow so that  $I_c^* > I_s^*$ . In this case, if  $I_s^* < I < I_c^*$ , then the dominance of the synchronous state decreases as  $\rho$  is increased and the cells can switch from an antisynchronous state to

a synchronous state by decreasing  $\rho$ . This implies that synchrony would be hindered by adding electrical coupling to an inhibitory network.

The above results imply that modulating the relative strengths of electrical and inhibitory coupling can alter the relative dominance of the synchronous and antisynchronous states. However, it is important to note that the results for the weak coupling limit imply that combining electrical coupling and inhibition does not promote synchrony over either electrical coupling alone or inhibitory coupling alone. That is, synchrony is most dominant either when  $\rho = 1$  (in the case of relatively fast inhibitory synapses and large spike effect) or when  $\rho = 0$  (in the case of relatively slow inhibitory synapses and a small spike effect) and never when  $0 < \rho < 1$ .

### 3.6. $\rho$ , $\alpha$ -Parameter Space

To further describe the effects of combined electrical and inhibitory coupling and for comparison to work

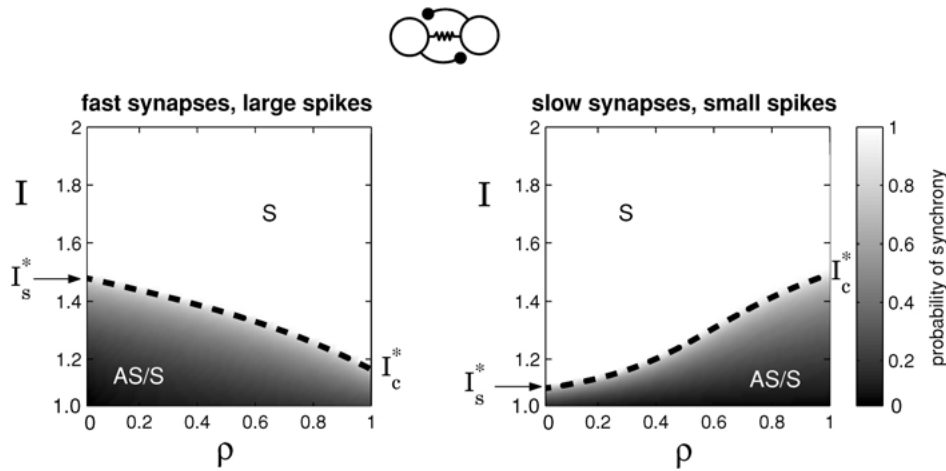


Figure 10. Two parameter response diagram for LIF cell-pair with combined electrical and inhibitory coupling,  $I, \rho$ -parameter space: This figure summarizes the main results of the paper.  $I_{sc}^*$  is the critical value of  $I$  above which only the synchronous state is stable (S) and below which both the synchronous and asynchronous states are stable (AS/S). The dashed lines plot the location of  $I_{sc}^*$  as a function of  $\rho$ , the fraction of total coupling due to electrical coupling.  $I_{sc}^* = I_s^*$  when  $\rho = 0$  and  $I_{sc}^* = I_c^*$  when  $\rho = 1$ .  $I_{sc}^*$  always changes monotonically with  $\rho$ . The grey-scale indicates the dominance of the synchronous state, i.e. the probability of the cells evolving to the synchronous state given a random initial phase difference between the cells. The panels depict two qualitatively different situations. (left) “Large” spike effect and “fast” inhibitory synapses,  $I_s^* > I_c^*$  ( $\beta = 0.3, \alpha = 4.0$ ). In this case, increasing the strength of the weak electrical coupling (increasing  $\rho$ ) promotes synchrony. (right) “Small” spike effect and “slow” inhibitory synapses,  $I_s^* < I_c^*$  ( $\beta = 0.1, \alpha = 1.5$ ). In this case, increasing the strength of the weak electrical coupling (increasing  $\rho$ ) promotes antisynchrony.

done on cells with inhibitory coupling alone (see Section 3.3 and van Vreeswijk et al. (1994)), it is useful to examine regions of synchrony and antisynchrony in the  $\rho, \alpha$ -parameter space. Figure 11 plots the location of the critical values of  $(\rho, \alpha)$  at which there are changes in stability of the asynchronous state (heavy dashed lines) for a fixed  $\beta$  and three values of  $I$  (increasing from top to bottom). In grey AS/S regions, stable synchronous and asynchronous states coexist, whereas in white S regions, only synchrony is stable. The overall effect of increasing  $I$  is to increase the S regime. This is consistent with the finding that synchronous activity is promoted by increases in the cells’ intrinsic frequency (described in earlier subsections).

For pure inhibitory coupling ( $\rho = 0$ ), there is a single critical value of  $\alpha$  below which only synchrony is stable and above which the synchronous and asynchronous states are both stable. This critical value of  $\alpha$  for inhibitory coupling alone increases as  $I$  increases (see Fig. 5). This suggests that cell-pairs can only exhibit asynchronous activity when inhibitory synapses have kinetics faster than a critical speed (van Vreeswijk et al., 1994). However, the top and middle panels of Fig. 11 reveal a rather counter-intuitive behavior. As  $\alpha$  decreases in the presence of electri-

cal coupling, the system goes from an AS/S region to a S region and then back to an AS/S region. That is, for sufficiently small  $I$ , electrical coupling allows stable asynchronous activity to exist when inhibitory synapses have very slow kinetics.

The explanation for this phenomenon is as follows. Electrical coupling alone at  $I = 1.2$  and  $\beta = 0.2$  supports both stable asynchronous and synchronous oscillations (see  $\rho = 1$  in Figs. 11 and 8). If  $\rho$  is relatively small, then the effects of inhibitory coupling will dominate and electrical coupling will be negligible for most values of  $\alpha$ . However, decreases in  $\alpha$  make the synaptic current smoother (more “tonic”), and although the synchronizing effect of inhibition is still there, it is substantially weaker than at higher values of  $\alpha$  when the synaptic current is more “phasic” (White et al., 1998). Therefore, for a given  $\rho$  and a sufficiently small  $\alpha$ , the influence of the electrical coupling effectively can dominate, enabling the existence of a stable asynchronous state.

Above  $I \sim 1.26$ , the asynchronous state is unstable for electrical coupling alone. Because electrical coupling does not promote antisynchrony for all  $I$  above this value, there is no longer a transition from the S region back to the AS/S region at small  $\alpha$ . An

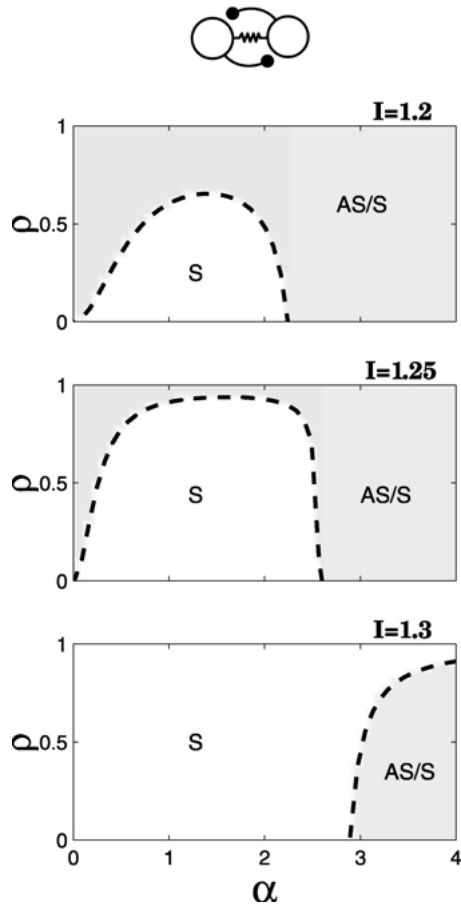


Figure 11. Two parameter response diagram for LIF cell-pair with combined electrical and inhibitory coupling,  $\rho$ ,  $\alpha$ -parameter space: The dashed lines plot the location of the transition points with spike effect held constant at  $\beta = 0.2$ . (top)  $I = 1.2$ , (middle)  $I = 1.25$ , (bottom)  $I = 1.3$ . For  $(\rho, \alpha)$  values in grey AS/S region, cells can exhibit either stable synchrony or antisynchrony; for  $(\rho, \alpha)$  values in white S region, cells can only exhibit stable synchrony. Note that, for  $I < I_c^*(\beta = 0.2) = 1.28$  and a range of  $\rho$ , as the speed of the synapse  $\alpha$  is decreased, the asynchronous state can lose stability and then regain stability at lower  $\alpha$  (see top and middle panels). This behavior cannot occur for inhibitory coupling alone,  $\rho = 0$ .

example of this is shown in Fig. 11 (bottom). In this case, the curve of critical values of  $(\rho, \alpha)$  monotonically increases, asymptoting to  $\rho = 1$ , with the AS/S region existing below the curve and S region existing above it.

The effects of varying the strength of the spike  $\beta$  with other parameters held constant can be examined in a similar fashion. However, it can be shown analytically that increasing  $\beta$  always promotes synchrony in the LIF model.

#### 4. Beyond Weak Coupling

The theory of weak coupling is only exact in the limit  $g_c, g_s \rightarrow 0$ , but it yields a good quantitative approximation when coupling strengths are sufficiently small. Furthermore, it is often found that the qualitative results from the weak coupling approximation persist for a surprisingly wide range of coupling strengths, as we demonstrate for the coupled LIF cells.

The full system, described by differential equations (5), is substantially harder to analyze than its weak coupling approximation. One could solve the full system numerically, but because the only nonlinearities in the LIF system are the threshold nonlinearities, analytical methods can be used to construct special solutions. When looking for phase-locked states, explicit solution formulae can be obtained for the activity between firings and then they can be patched together across firings. This reduces the differential equation system to a system of two algebraic equations for the unknown period  $T$  and phase difference  $0 \leq \phi \leq 1$  (van Vreeswijk et al., 1994; Chow, 1998; Bressloff and Coombes, 2000; Chow and Kopell, 2000).

Assume that the cells are firing periodically with period  $T$  and that cell 1 fires at times  $t = nT$  while cell 2 fires at times  $t = (n + \phi)T$  (for any integer  $n$ ). This assumption imposes the following ‘‘matching’’ conditions on the membrane potentials of cell 1 and cell 2,  $v_1$  and  $v_2$ . At time  $t = 0$ ,  $v_1$  reaches threshold  $v_{TH} = 1$ , cell 1 fires and  $v_1$  is reset to 0. If  $v_2 = u_2$  just before cell 1 fires, then  $v_2 = u_2 + g_c\beta$  immediately after the spike in cell 1. Similarly, just before cell 2 fires at  $t = \phi T$ ,  $v_2$  is 1 and we can take  $v_1 = u_1$ . Immediately following the spike of cell 2, cell 2 is reset to 0 and the spike effect is added to cell 1 so that  $v_1 = u_1 + g_c\beta$ . Finally, just before cell 1 fires at  $t = T$ ,  $v_1$  is 1, and for there to be a  $T$ -periodic solution,  $v_2 = u_2$ . In summary,

$$\begin{aligned} v_1(0^-) &= 1, & v_2(0^-) &= u_2, \\ v_1(0^+) &= 0, & v_2(0^+) &= u_2 + g_c\beta, \\ v_1(\phi T^-) &= u_1, & v_2(\phi T^-) &= 1, \\ v_1(\phi T^+) &= u_1 + g_c\beta, & v_2(\phi T^+) &= 0, \\ v_1(T^-) &= 1, & v_2(T^-) &= u_2. \end{aligned}$$

Equations (5) can be integrated analytically to get a general solution for  $v_1(t)$  and  $v_2(t)$  that is valid for  $0 < t < \phi T$  and  $\phi T < t < T$ . It is convenient to work with the transformed variables  $v_+ = v_1 + v_2$  and  $v_- = v_1 - v_2$ . Using the general solution and the matching conditions, we obtain a set of four algebraic

equations for  $u_1, u_2, T$  and  $\phi$ .

$$\left\{ \begin{array}{l} u_1 - \beta g_c + 1 = u_2 e^{-\phi T} + 2I(1 - e^{-\phi T}) \\ \quad + g_s \left[ e^{-T} \int_{(1-\phi)T}^T e^t s_T(t) dt \right. \\ \quad \left. + e^{-\phi T} \int_0^{\phi T} e^t s_T(t) dt \right] \\ u_1 - \beta g_c - 1 = -u_2 e^{-\phi T} \\ \quad + g_s \left[ e^{-\mu T} \int_{(1-\phi)T}^T e^{\mu t} s_T(t) dt \right. \\ \quad \left. - e^{-\mu \phi T} \int_0^{\phi T} e^{\mu t} s_T(t) dt \right] \\ 1 + u_2 - \beta g_c = u_1 e^{-(1-\phi)T} + 2I(1 - e^{-(1-\phi)T}) \\ \quad + g_s \left[ e^{-(1-\phi)T} \int_0^{(1-\phi)T} e^t s_T(t) dt \right. \\ \quad \left. - e^{-T} \int_{\phi T}^T e^t s_T(t) dt \right] \\ 1 - u_2 + \beta g_c = u_1 e^{-\mu(1-\phi)T} \\ \quad + g_s \left[ e^{-\mu(1-\phi)T} \int_0^{(1-\phi)T} e^{\mu t} s_T(t) dt \right. \\ \quad \left. - e^{-\mu T} \int_{\phi T}^T e^{\mu t} s_T(t) dt \right] \end{array} \right.$$

where  $\mu = 1 + 2g_c$ . The integrals involving the periodic synaptic current  $g_s s_T(t)$  are easily evaluated analytically. Also,  $u_1, u_2$  can be easily eliminated to produce a set of two algebraic equations for  $T$  and  $\phi$ .

Most solutions to this algebraic system correspond to 1:1 phase-locked behavior of the coupled cell system with phase difference  $\phi$ . However, there are exceptions. Some solutions to the algebraic system require that membrane potentials exceed the threshold for firing. These solutions do not correspond to “physical” behaviors of the system, but they imply the existence of the dynamical states of “spike-capture synchrony” or suppression, which do not occur in the case of weak coupling. Suppression (White et al., 1998) occurs when inhibition is so strong that one cell’s repetitive firing inhibits the other cell so much that the inhibited cell never fires. “Spike-capture synchrony” occurs as follows. If a cell has a membrane potential of  $u$  such that  $1 - g_c \beta < u < 1$  immediately before the other cell fires, the cell will be knocked above threshold by the

spike ( $u + g_c \beta > 1$ ), and therefore the cells will immediately synchronize.

Solutions to the algebraic system are nonphysical when they have  $u_1$  or  $u_2 > 1 - g_c \beta$  and  $\phi \neq 0, 1$ . (Recall that  $u_1$  and  $u_2$  are membrane potentials of cell 1 and 2 immediately before spike effects are added). This happens for low  $I$  (low intrinsic frequencies) where the approach to threshold is slow and cells remain close to threshold for a long time before firing. The range of  $I$  over which spike-capture synchrony and suppression occur in place of solutions to the algebraic system increase as  $g_c \beta$  and  $g_s$  increase, respectively. However, the range of  $I$  over which this occurs is only substantial when coupling strengths are quite large.

The depolarizing effect of the spike ensures that the synchronous state for non-weak coupling is always stable. If initial conditions are close enough, then when one cell fires the other will immediately fire and the cells will be exactly synchronized, i.e. synchrony is achieved by spike-capture synchrony mechanism. On the other hand, when the effect of the suprathreshold portion of the spike is not present ( $\beta = 0$ ), the synchronous state can lose stability. For inhibition alone, this loss of stability is associated with a transition to suppression; it occurs when inhibition is sufficiently strong and slow and  $I$  is sufficiently small (Bressloff and Coombes, 2000).

Using the spike response method (Gerstner, 1995) or an equivalent method, the stability of phase-locked states in the case of non-weak coupling can be found by constructing an extension of the  $G$ -function that was defined for the weak coupling limit (Chow and Kopell, 2000; Chow, 1998; van Vreeswijk et al., 1994). Also, it may be possible to extend the work of Bressloff and Coombes (2000) and investigate stability of the asynchronous states by constructing a linearized map of firing times and analyzing its spectrum. However, the combination of the electrical and inhibitory coupling makes both of these methods algebraically complicated. We therefore choose to simply infer stability by comparing with the weak coupling results and checking stability for representative phase-locked states using numerical simulations.

Unlike the weak coupling case, it is hard to make definitive statements regarding the dependence of phase-locked states on parameters. Our approach is to numerically solve the algebraic system for various parameter sets, look for trends, and compare results with those for weak coupling. Fortunately, the only qualitative differences between the weak coupling theory

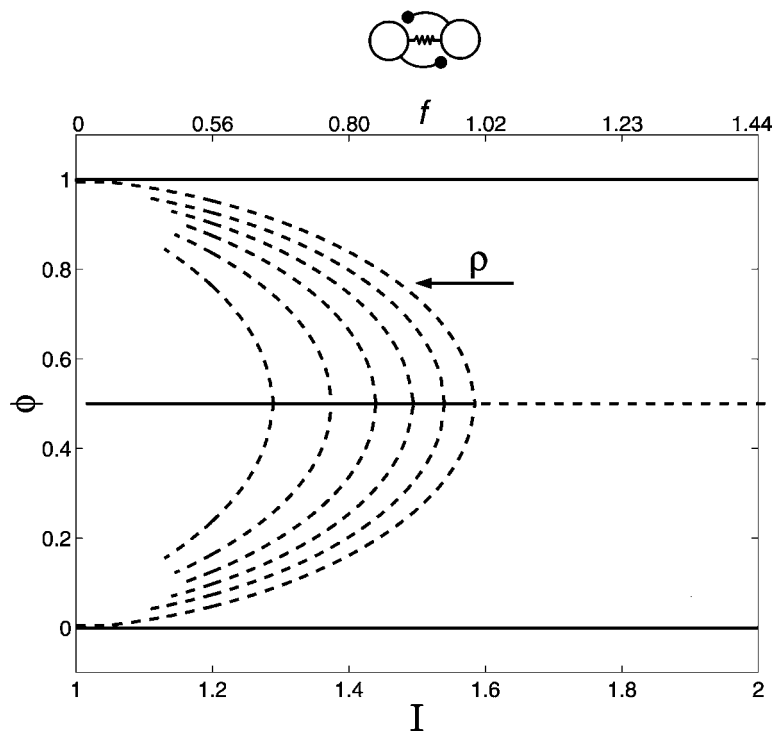


Figure 12. Results without the weak coupling approximation: Bifurcation diagrams for LIF cell-pair with fixed total coupling strength  $g_{tot} = g_s + g_c = 0.1$ ,  $\alpha = 4.0$ ,  $\beta = 0.2$  and various ratios of electrical and inhibitory coupling. The overlaid bifurcation diagrams shift systematically with  $\rho$ . From right to left,  $\rho = 0, 0.2, 0.4, 0.6, 0.8, 1$ . The “tines of the forks” in the bifurcation diagrams corresponding to asynchronous phase-locked states cease to exist at low values of  $I$ . This is due to spike-capture synchrony or suppression. The values of  $I$  below which the asynchronous states do not exist depend on  $\rho$ . This is seen on the tines corresponding to unstable asynchronous-non-antisynchronous states, but it is obscured for antisynchronous state  $\phi = 0.5$  due to the overlaying of the bifurcation diagrams.

results and results beyond weak coupling are those mentioned above, i.e. the presence of suppression and spike-capture synchronization.

Figure 12 portrays overlaid bifurcation diagrams,  $\phi$  vs  $I$ , for solutions to the algebraic systems for various values of  $\rho$  and with fixed values of  $\alpha$ ,  $\beta$  and total coupling strength  $g_{tot} = g_c + g_s$ . The non-physical solutions are omitted. For all  $\rho$ , synchronous and antisynchronous states exist at large values of  $I$  (high intrinsic frequency), but only the synchronous state is stable. As  $I$  decreases through a critical value, a subcritical pitchfork bifurcation occurs where the antisynchronous state becomes stable. Furthermore, the critical values of  $I$  change monotonically with  $\rho$  and remain between the critical values for electrical coupling alone or inhibitory coupling alone. Qualitatively, the phase-locking structure is the same as that given by the weak coupling approximation. The sole qualitative difference is that the three “tines of the forks” of the bifurcation diagrams corresponding to asynchronous phase-locked states, including the stable an-

tisynchronous states, cease to exist at low values of  $I$ . As explained above, this is due to spike-capture synchrony or suppression. The values of  $I$  below which the asynchronous states cease to exist depend on  $\rho$ . This is seen on the branches corresponding to unstable asynchronous-non-antisynchronous states, but it is obscured on the branches corresponding to antisynchronous state due to the overlaying of several bifurcation diagrams.

Figure 13 shows how the phase-locking structure depends on the strength of the coupling. This example fixes  $\rho = 0.5$  but the structure appears to be qualitatively similar for all  $\rho$ . As the total coupling strength  $g_{tot} = g_c + g_s$  increases, the bifurcation point shifts to higher values of  $I$  and the stable antisynchronous state persists for a larger  $I$ . This trend was also observed for electrical coupling alone by Chow and Kopell (2000). As  $g_{tot}$  is increased, the effect of the spike is larger, which increases the likelihood of spike-capture synchrony, and tendency for suppression also increases. This causes the tines of the forks in the bifurcation

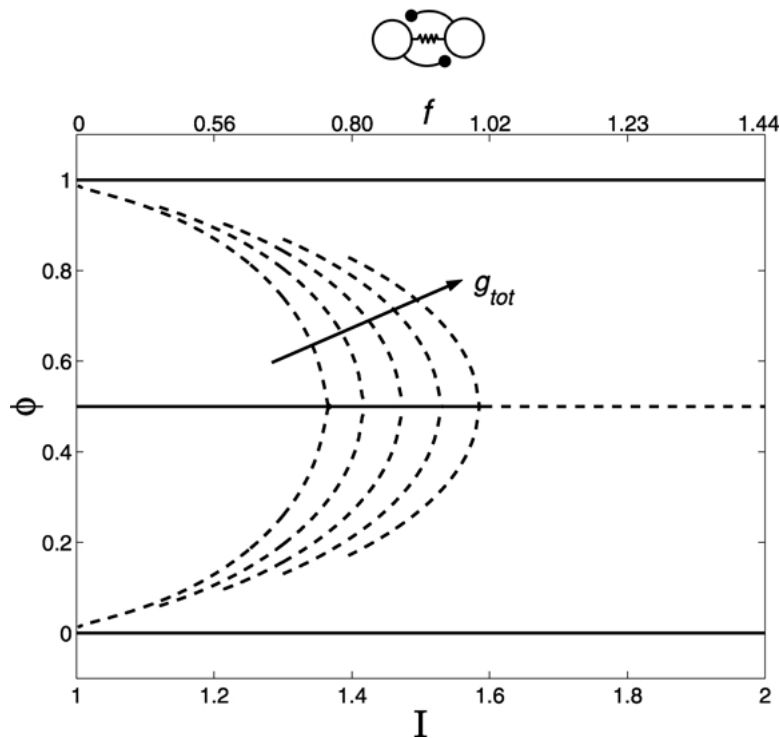


Figure 13. Results without the weak coupling approximation: Bifurcation diagrams for LIF cell-pair with various total coupling strength and a fixed ratio of electrical and inhibitory coupling  $\rho = 0.5$  ( $\alpha = 2.0$ ,  $\beta = 0.1$ ). From left to right: the weak coupling limit,  $g_{tot} = 0.1, 0.2, 0.3$  and  $0.4$ ). The critical values of  $I$  and unstable states for the combined coupling case increase systematically as  $g_{tot}$  is increased. As a result of spike-capture synchrony and suppression, the “tines of the forks” in the bifurcation diagrams corresponding to asynchronous phase-locked states cease to exist at low values of  $I$ . The values of  $I$  below which the asynchronous states do not exist depend on  $g_{tot}$ . This dependence is obscured for antisynchronous state  $\phi = 0.5$  due to the overlaying of the bifurcation diagrams.

diagram to get shorter, corresponding to an increase in the range of  $I$  over which the unstable asynchronous states and stable antisynchronous states cease to exist. Note that the effect is present for all three tines of the forks in the bifurcation diagrams but the effect for  $\phi = 0.5$  is hidden by the overlays for various  $\rho$ .

In the weak coupling limit, the period of oscillation of the coupled cells is always the same as the intrinsic period of the uncoupled cells. Away from this limit, the period of the phase-locked states can differ from the period of the uncoupled cells. Increasing the strength of inhibition always increases the period of synchronous and antisynchronous activity. Increasing the strength of electrical coupling can either increase or decrease the period of the antisynchronous state, but it does not affect the period of the synchronous state (Chow and Kopell, 2000). When both the antisynchronous and synchronous states exist, they can sometimes have very different periods.

## 5. Discussion

In this paper, we study a model of two identical leaky integrate-and-fire (LIF) cells connected by electrical coupling and reciprocal inhibition. The idealized formulation of the model has enabled us to begin to construct a framework for understanding how the combination of electrical and inhibitory coupling affects synchronization patterns in networks of spiking neurons. The results of our study are summarized in Table 1 and in the text.

### 5.1. Results for Weak Coupling

Most of our work on the two cell system is done in the limit of weak coupling, where the theory of weakly coupled oscillators allows extensive analysis over a broad range of parameters. The analysis shows that the intrinsic frequency of the cells, which is controlled by

*Table 1.* Summary of results for LIF model.

Parameter variation	Effect
Increasing intrinsic frequency ( $\uparrow I$ )	Promotes synchrony
Increasing fraction of coupling due to electrical coupling ( $\uparrow \rho$ ), with	
Fast synapses, large spike effect ( $I_c^* > I_s^*$ )	Promotes synchrony
Slow synapses, small spike effect ( $I_c^* < I_s^*$ )	Promotes antisynchrony
Increasing spike effect ( $\uparrow \beta$ )	Promotes synchrony
Increasing speed of synapse ( $\uparrow \alpha$ ), with	
Sufficiently high frequency ( $I > I_c^*$ )	Promotes antisynchrony
Sufficiently low frequency ( $I < I_c^*$ )	Can promote synchrony when synapses are sufficiently slow
Increasing total coupling strength ( $\uparrow g_{tot}$ )	Promotes synchrony or suppression; can promote antisynchrony around the critical frequency

the level of applied constant current, has a characteristic influence on synchronization properties. For electrical coupling alone or inhibitory coupling alone, only synchronous behavior is stable when the intrinsic frequency is high. Below a critical frequency, the coupled-cell system supports both stable synchronous and antisynchronous activity. This bistability persists for all intrinsic frequencies below the critical frequency, but synchronous behavior dominates close to the critical frequency and antisynchrony increases in dominance as intrinsic frequency decreases. That is, given a random initial phase difference between the cells, the probability that the system evolves to the synchronous state is approximately one when the intrinsic frequency of the cells is close to the critical frequency, and this probability decreases as the intrinsic frequency is decreased, eventually becoming close to zero. Thus, for the LIF model, both inhibition alone and electrical coupling alone promote synchrony when the intrinsic firing rate of cells is high, antisynchrony when the firing frequency is low, and bistability in an intermediate frequency range (Figs. 4 and 7).

For combinations of electrical and inhibitory coupling, the effects of the two coupling modes add linearly in the weak coupling limit. Because the phase-locking behaviors of the two coupling modes are qualitatively the same, the general trends for combined coupling are the same as those for the cases of either coupling mode alone: synchrony is promoted at high intrinsic frequencies and antisynchrony or bistability is promoted at lower frequencies.

For a small spike effect and relatively slow synapses, the critical frequency for inhibition alone is smaller

than that for electrical coupling alone. For a large spike effect and relatively fast synapses, the critical frequency for inhibition alone is greater than that for electrical coupling alone. The critical frequencies for combined coupling are necessarily intermediate to those for the single coupling modes alone. In fact, there is a monotonic relationship between critical frequency and  $\rho$ , the fraction of coupling due to electrical coupling. (see Figs. 9 and 10). This is also the case for the relative dominance of antisynchrony and synchrony in the bistable regime (Figs. 9 and 10). For a fixed intrinsic frequency, the probability of synchrony changes monotonically as  $\rho$  increases. Increasing electrical coupling promotes synchrony when synapses are relatively fast and the spike effect is sufficiently large, but it promotes antisynchrony when synapses are relatively slow and the spike effect is sufficiently small.

The above observations imply that electrical coupling and inhibitory coupling do not act synergistically to promote synchrony. Either electrical coupling alone or inhibitory coupling alone, not a combination of the two, is best for promoting synchronous activity. The same is true for promoting antisynchrony. Note that these statements are in a specific context, where “promoting synchrony” is defined as “increasing the probability of synchronous activity given random initial conditions.” Also, because we deal with identical cell-pairs without noise, our results will hold for cases where cells are sufficiently homogeneous and noise is sufficiently small. However, the results are inconclusive for cases with large heterogeneity and large amounts of noise.

For mutual inhibition alone, the critical value of the intrinsic frequency where stability of the

antisynchronous state changes depends on the speed of the inhibitory synapses,  $\alpha$ : Faster synapses move the critical frequency to higher values, allowing antisynchrony to persist over a broader range of frequencies (Fig. 5). For electrical coupling alone, the critical value changes with the magnitude of the direct electrotonic effect of the spikes,  $\beta$ : When the spike effect increases, the critical frequency decreases, extending the range of frequencies over which only synchronous activity exists. (Fig. 8). For any fixed combination of inhibitory and electrical coupling, increasing the strength of the spike effect always decreases the critical frequency, thus stronger spikes always promote synchrony. Increasing the speed of the synapses promotes antisynchrony at sufficiently high intrinsic frequencies. However, when frequencies are sufficiently low, increasing the speed of the synapse can actually promote synchrony (Fig. 11).

In this paper, current-based  $\alpha$ -synapses are explicitly used rather than conductance-based  $\alpha$ -synapses. Spike-triggered postsynaptic currents of conductance-based  $\alpha$ -synapses are described by

$$I_{syn,jk} = g_{syn}\alpha^2 t e^{-\alpha t} (V_j - V_{syn}),$$

where  $g_{syn}$  scales the synaptic conductance and  $V_{syn}$  is the reversal potential of the synaptic current. Conductance-based  $\alpha$ -synapses are often considered more realistic than the current-based  $\alpha$ -synapses. However, for the LIF model in the weak coupling limit, the  $G$ -functions for cells coupled by conductance-based  $\alpha$ -synapses differ from those for cells coupled by current-based  $\alpha$ -synapses only by the scaling factor  $g_{syn}/q_s(V_{syn} - I)$ . Thus, phase-locked states for cells coupled by conductance-based  $\alpha$ -synapses are identical to those discussed in this paper. Note that shunting inhibition ( $V_{syn} \sim$  resting potential) is not a special situation in the case of weakly coupled oscillating LIF cells.

### 5.2. Effects of Coupling Strength

The results for weak coupling are quantitatively accurate for sufficiently small coupling strengths ( $g_c$  and  $g_s$ ), but the qualitative results extend over a wide range of coupling strengths. In the limit of weak coupling, changes in  $g_c$  and  $g_s$  can change the phase-locking behavior, but only if there are changes in  $\rho$ , the ratio of  $g_c$  to  $g_{tot} = g_c + g_s$ . Otherwise, the strengths of the coupling do not play roles in determining the phase-

locked states or the linear stability of these states (as is true for cells connected by a single coupling mode). The coupling strengths do however effect the speed at which cells converge to or diverge from the phase-locked states. The rate at which weakly coupled oscillators converge to phase-locked states is inherently slow. The rate of convergence is of the order  $g_{tot}/T$ . That is, the cells take on the order of  $1/g_{tot}$  cycles to appear phase-locked. Thus, if  $g_{tot} \sim 0.01$ , then hundreds of cycles are needed to attain synchrony or antisynchrony, but if  $g_{tot} \sim 0.1$ , only tens of cycles are required (see Figs. 1 and 2).

For moderate coupling strengths (i.e. away from the limit of weak coupling), coupled cell systems are more difficult to study, but some analytical results can still be obtained for LIF cells (see Section 4, van Vreeswijk et al., 1994; Chow, 1998; Chow and Kopell, 2000; Bressloff and Coombes, 2000). When coupling is not weak, the strengths of the coupling,  $g_c$  and  $g_s$ , have some effect on the phase-locking structure. As coupling strength increases, there is a rightward shift in the bifurcation diagrams that extends the range of frequency over which a stable antisynchronous state exists (see Fig. 13). Qualitatively, however, the locking structure remains the same except for a few minor features. When inhibition or electrical coupling is sufficiently strong, suppression or spike-capture synchronization can occur. The effects of these phenomena on the phase-locking structure are seen at low frequencies and are minimal unless coupling is quite strong.

### 5.3. Direct Effect of the Spikes

The results presented here and the previous results of Chow and Kopell (2000) show that spikes can play a large role in determining the existence and the stability of phase-locked states when cells are electrically coupled. However, the effects of spikes in the two studies are modeled in different ways. Chow and Kopell (2000) model the action potential by imposing a brief inward current on a cell when it reaches a threshold potential. This inward current is applied for a specified duration (the spike width) and is followed by an infinitely fast reset to a reset potential. We model the effect of the suprathreshold portion of a spike by lumping all electrotonic current flowing from a spiking cell to a subthreshold cell into a  $\delta$ -function current. An important condition for this to be a reasonable approximation is that the width of a spike is much smaller than the period of the oscillations.

Our model makes analytical calculations less complicated than those for the formulation of Chow and Kopell, and it captures the phase-locking structure and its dependence on parameters seen by Chow and Kopell for all but ultra-high frequencies, i.e. when the period of the oscillations is less than twice the spike width. At ultra-high frequencies, Chow and Kopell found that synchrony can become unstable and asynchronous states can become stable. Chow and Kopell confirmed that changes in stability occur at high frequencies in two conductance-based neuronal models (White et al., 1998; Ermentrout and Kopell, 1998). These findings of Chow and Kopell could be important in understanding 200 Hz ripple activity in hippocampus (Ylinen et al., 1995). The only concern is that the phase-locked states seen at high frequencies may not be robust to noise and heterogeneities (as will be explained below).

The models presented here and in Chow and Kopell are single-compartment models, and they neglect the filtering effects of dendrites on phase-locking (Crook et al., 1998; Bressloff and Coombes, 1997). Preliminary evidence suggests that gap junctions between cortical interneurons are located on somata and proximal dendrites (Tamás et al., 2000). Based on this evidence, it is likely that dendritic effects can be neglected. However, if electrical coupling were sufficiently far out on the dendrites, then the current that one cell experiences due to a spike in the other cell could be broadened enough to substantially alter the stability of phase-locked states, and therefore synchrony could become unstable and asynchronous states could become stable when the period of the oscillations is considerably greater than the spike width, i.e. not only at ultra-high frequencies. Indeed, Alvarez et al. (2002) studied a model in which pairs of cells were electrically coupled via dendrites and showed that a transition from stable synchrony to stable antisynchrony can occur when intrinsic frequency is increased. They also showed that this could be applicable to electrically coupled cells in the locus coeruleus.

#### 5.4. *Cortical Interneurons*

Although the population of cortical interneurons is extremely diverse (Gupta et al., 2000), they have been divided into two major groups, fast-spiking (FS) cells and low-threshold spiking (LTS) cells (Gibson et al., 1999). FS cells have narrow action potentials each with a deep, brief after-hyperpolarization, and they can fire at high frequencies with little or no spike-frequency adapta-

tion (Gibson et al., 1999; Galarreta and Hestrin, 1999; Erisir et al., 1999); LTS cells have slightly broader action potentials, shallower after-hyperpolarization and pronounced spike-frequency adaptation (Gibson et al., 1999; Beierlein et al., 2000).

Recently, experimentalists have used in vitro paired-cell recordings to assess the connectivity between cortical neurons (Gibson et al., 1999; Galarreta and Hestrin, 1999; Amitai et al., 2002). (See Fig. 1 in Beierlein et al. (2000) for a schematic connectivity diagram.) Results indicate that there is a high degree of inhibitory connectivity between FS cells, whereas inhibitory connections between LTS cells are rare. Furthermore, FS cells display extensive electrical coupling between one another. The same is true for LTS cells. However, there is very little electrical connectivity between FS cells and LTS cells. This suggests that interneurons could be separated into at least two functional inhibitory networks. The different functions of these networks remain unclear, but the different intrinsic properties and connectivities of the networks are likely to be tuned to perform these functions. It therefore is important to examine how these aspects influence network dynamics.

Paired-cell recordings in brain slice preparations provide a simple way to begin studying the dynamical interactions between interneurons. There is usually very little spontaneous activity in resting neocortical slices. A cell in the slice fires only when a sufficient amount of depolarizing current is applied to it. Cells in a cell-pair may be electrically connected to other cells in the network (Amitai et al., 2002). However, because coupling is fairly weak and unstimulated cells are far below threshold, the coupling current due to the load of these unstimulated cells should act like an extra leakage current with a reversal potential equal to the resting membrane potential of the unstimulated cells. Furthermore, inhibitory synaptic interactions do not lead to any feedback input from outside the cell pair. Therefore, the cell-pair is effectively isolated from the rest of the network, and thus the paired-cell system is a direct experimental analog for the two-cell model considered in this paper.

Despite the LIF model being idealized, we expect that the qualitative results described here will carry over to FS and LTS cell-pairs and conductance-based models of these cell-pairs. The results for the LIF model predict that connected cells will fire antisynchronously at low levels of applied constant current, and they will display synchronous activity at high applied current. A region of bistability is predicted to exist

in an intermediate range of applied constant current. We also predict that modulating the relative strengths of electrical coupling and inhibition can cause changes in phase-locking states in certain frequency ranges. However, determining exactly where FS or LTS cells fit into our LIF-based framework may not be a straightforward task. Unlike the LIF model, FS and LTS cells cannot fire at arbitrarily high frequencies in response to applied constant currents, and FS cells cannot fire at arbitrarily low frequencies (Erisir et al., 1999). Therefore, coupled cells do not necessarily exhibit all of the qualitative behavior that LIF cell-pairs exhibit.

When injected with constant current, many neurons, including LTS interneurons, can fire at arbitrarily low frequencies. These neurons are said to have type-I excitability (Rinzel and Ermentrout, 1998; Ermentrout, 1996). All real neurons and conductance-based models have maximal firing frequencies. If a pair of LTS cells or any other type I neurons exhibits only synchronous activity at their maximal frequency, we would expect to see a transition to antisynchrony at lower frequencies. On the other hand, if inhibitory synapses are sufficiently fast or the direct effect of the spike is sufficiently small, then it is possible that the asynchronous state would dominate over the entire frequency range.

Some neurons are not capable of firing at arbitrarily low frequencies in response to constant applied current. Instead, the cells have a characteristic minimal frequency for a critical current amplitude, and below this critical current amplitude, they do not fire. Neurons that display this behavior, such as FS cells (Erisir et al., 1999), are said to have type-II excitability (Rinzel and Ermentrout, 1998). Type-II cell-pairs could exhibit the same types of behavior described in the previous paragraph for the type-I cell-pairs. However, if a type-II cell-pair with fixed coupling exhibits only synchronous activity at the minimal frequency, then we would predict that synchrony would prevail over the entire frequency range. Theoretically, this behavior cannot occur in type-I neurons for sufficiently weak coupling. Because type-I cells can fire at very low frequencies, they should always be able to exhibit asynchronous activity over some range of low  $I$ . Note however that for strong coupling, suppression or synchrony via the spike-capture mechanism could wipe out this regime of antisynchrony.

As of yet, no experimental study has systematically examined the dependence of phase-locked patterns of cell-pairs on intrinsic frequency or other cell properties or network parameters. We expect that the results

presented here will be applicable to FS and LTS cell pairs. The LIF model may provide a better representation of FS cells than of LTS cells, because FS cells have especially thin spikes. Preliminary results using a conductance-based model of FS cells and in vitro cell-pair recordings agree with those presented here (Lewis et al., 2001).

In vitro FS cells have membrane time constants in the range of 5–10 ms. Let us suppose that the membrane time constant is 8 ms. The dimensionless frequency range shown in our figures (0–1.44) would then correspond to 0–180 Hz. For inhibitory coupling alone, if the time constant of the  $\alpha$ -function postsynaptic current is  $\sim 4$  ms, then our results predict that the critical frequency for stability of the asynchronous state would be  $\sim 70$  Hz. This agrees with the initial experimental studies (Lewis et al., 2001). Electrically coupled FS cells appear to exhibit only synchronous activity at their minimal frequencies (Lewis et al., 2001). According to our results, adding electrical coupling to a cell-pair connected by inhibition should therefore decrease the critical frequency and promote synchrony. This also agrees with the initial experimental findings (Lewis et al., 2001). In vitro FS cell-pairs appear to fit into the framework for cells with a strong spike effect and relatively fast synapses, displaying activity similar to those depicted in Fig. 10 (left).

### 5.5. The Role of Combined Coupling

Recently, Tamás et al. (2000) presented experimental evidence that suggests that the inhibition and electrical coupling in interneuronal networks could act synergistically to promote neuronal synchronization. They studied gamma-frequency ( $\sim 40$  Hz) phase-locking in pairs of interneurons in vitro. They found that unitary GABAergic connections were ineffective for phase-locking and electrical coupling produced phase-locking with substantial phase-lags, whereas combined electrical and GABAergic synaptic coupling synchronized cells with no apparent phase-lag.

In the context of our definition of “promoting” synchrony, the results of Tamás et al. appear to contradict the results that we present here. However, although both studies consider pairs of oscillating cells with either inhibitory coupling alone, electrical coupling alone or combinations of the two coupling modes, there are fundamental differences between the system that we consider and the system that Tamás et al. considered.

Firstly, the inhibitory coupling between cell-pairs in the Tamas et al. study was only one-way, whereas our model has reciprocal inhibition. Secondly, using current injection, the cells in the study of Tamas et al. were made to fire with widely disparate intrinsic frequencies. The presynaptic cell was made to intrinsically fire at  $\sim 40$  Hz and the postsynaptic cell was made to intrinsically fire at  $\sim 5$  Hz. The interaction between the cells either reduced or increased the frequency of the postsynaptic cell only slightly. Thus, the synchrony that they refer to could be classified as  $\sim 10 : 1$  phase-locking, i.e. on average, the postsynaptic cell fires only once for every 10 spikes in the presynaptic cell. Our reciprocally inhibited cells fire with similar or the same intrinsic frequencies; the rhythms that we consider are  $1 : 1$  (or  $1 : 0$ ) phase-locked rhythms.

Together the results of Tamas et al. and our results imply that it may be possible that combined coupling enhances synchrony in certain situation, but this appears not to be a general rule (see Fig. 11). More work needs to be done to extend our framework to include strongly heterogeneous intrinsic properties and coupling properties. This work would include the situation studied in Tamas et al. as a special case.

Throughout the paper, we have defined “promoting synchrony” as “increasing the probability that the cells will evolve to a synchronous state given random initial conditions.” This is perhaps the only reasonable definition for the homogeneous deterministic system that we consider. However, neuronal networks are inherently noisy and have heterogeneous connectivity and cellular properties. These features can lead to the destruction of synchrony or other phase-locked states. Therefore, a definition of “promoting synchrony” should also include reference to “increasing the robustness of synchrony.”

The effect of heterogeneity in intrinsic frequency has been studied in models of large neuronal networks with inhibitory coupling alone (White et al., 1998; Wang and Buzsáki, 1996). These studies have shown that synchrony is fragile even in the presence of mild heterogeneity when the frequency is sufficiently high or low with respect to the speed of the inhibitory synapses. At low frequencies, this lack of robustness could be due to the presence of the stable antisynchronous state or subharmonic phase-locked states or due to the presence of suppression for sufficiently strong inhibition (White et al., 1998). At high frequencies, the net inhibitory current is effectively smoothed out (i.e. it is more “tonic”), and therefore synchronizing forces are

low, and synchrony is less robust to the heterogeneity (White et al., 1998). Similar results should hold for the addition of membrane noise instead of or on top of heterogeneity.

Increasing the inhibitory coupling strength,  $g_s$ , will initially increase the robustness of inhibition-induced synchrony. This is easy to see in the weak coupling limit. Sufficiently weak heterogeneities and noise can be accounted for by additional terms on the right-hand side of the differential equation for  $\phi$  involving  $G_s(\phi)$  (Eq. (8)). The magnitude of  $G_s(\phi)$  measures the overall strength of the dynamics of the homogeneous noiseless system. That is, it not only determines the rate at which the system converges to the phase-locked states, but it also determines how large perturbations to the system (due to heterogeneities or noise) must be in order to substantially affect the dynamics. If the magnitude of  $G_s(\phi)$  is large, then large amounts of noise or high degrees of heterogeneities are needed to destroy phase-locked behavior. However, if the magnitude of  $G_s(\phi)$  is small, then phase-locked states can be destroyed by mild heterogeneity and small amounts of noise. Note that  $g_s$  scales the magnitude of  $G_s(\phi)$ . This implies that the robustness of phase-locked states increases with synaptic strength just as long as it is not strong enough to induce suppression.

It has been suggested that the presence of electrical coupling in inhibitory networks could help to make synchronous activity more robust (White et al., 1998; Chow and Kopell, 2000; Traub et al., 2001). At low frequencies, whether this holds or not depends on the intrinsic dynamics of the cells, which determine whether or not electrical coupling has a synchronizing or desynchronizing effect. At higher frequencies, electrical coupling tends to synchronize, and therefore adding electrical coupling should increase the robustness of synchronous activity. However, because inhibition acts to synchronize activity at high frequencies, increasing the strength of the weak inhibitory coupling can do this as well.

Above a certain frequency, increases in the intrinsic frequency of the cells lead to decreases in the magnitude of  $G_s(\phi)$ . This implies that phase-locked states in inhibitory networks can be fragile at high frequencies and can be destroyed relatively easily by mild heterogeneity or low levels of noise, which is consistent with the modeling results mentioned above (White et al., 1998; Wang and Buzsáki, 1996). A similar result holds for electrically coupled cells. At high enough frequency,  $G_c(\phi)$  decreases with increased intrinsic

frequency, and therefore synchrony mediated by electrical coupling at high frequency is fragile. Because the  $G$ -function for combined electrical and inhibitory coupling is simply the sum of  $G_c(\phi)$  and  $G_s(\phi)$ , synchrony mediated by combined coupling has the same property.

Recently, Traub and colleagues (2001) have simulated the activity of large networks of physiologically-realistic model interneurons, studying their synchronization properties at  $\sim 40$  Hz. They found that there was a sharp threshold for electrical coupling strength above which cells in the network synchronize their activity but below which cells fire asynchronously. This is what would be predicted from the results here if there are fixed initial conditions. At  $\sim 40$  Hz, the interneurons do not synchronize. As electrical coupling strength is increased,  $\rho$  increases. The asynchronous activity is maintained until a critical value of  $\rho$  at which point the initial condition switches from the basin of attraction of the asynchronous state to the basin of attraction of the synchronous state. The cells in the network would synchronize for  $\rho$  above this critical value. We would predict that the critical value of  $\rho$  would vary with the set of initial conditions used.

Other roles for combinations of electrical and inhibitory coupling in neuronal networks have been suggested. One hypothesis is that it serves to generate stable bursting patterns (Skinner et al., 1999). Also, modeling work on inhibitory networks of cells with broad plateau potentials has demonstrated that the presence of strong electrical coupling in the embryonic lobster stomatogastric nervous system could serve to mask the large amplitude antisynchronous activity that is seen in adults (Bem et al., 2002). The LIF model considered here cannot address these issues specifically, because the LIF cells have no plateau potentials and there are no mechanisms for bursting in the model.

In this study, we have assumed that interneurons are in an oscillatory mode. It is possible that combined coupling plays a larger role in processing transient or randomly fluctuating input (Galarreta and Hestrin, 2001b; Swadlow et al., 1998). Because electrical coupling is subthreshold coupling (as well as suprathreshold coupling), it could promote strong synchronous firing when input to the cells is correlated and diminished responses when input is decorrelated (via mutual shunting) (Galarreta and Hestrin, 1999; Galarreta and Hestrin, 2001b; Usher et al., 1999). The recurrent inhibition is only suprathreshold coupling and would only be induced after the cells fire. Thus, inhibition could be

present simply to abruptly quench activity in the network or it could act to sharpen the above effect of the electrical coupling by further diminishing the response to decorrelated input.

The work presented here begins to construct a framework for understanding how the combination of electrical and inhibitory coupling can shape the activity in a neuronal network. All results in the paper were obtained using a model with leaky integrate-and-fire cells and idealized coupling. Thus, in order to solidify the applicability of the results, it is essential to perform further systematic experiments in brain slice preparations, as well as carry out extensive numerical simulations on conductance-based models with more realistic synaptic dynamics. Also, this work should be extended to include large networks, explicitly studying the effects of connectivity structure, heterogeneities and noise and eventually the interactions with excitatory cells and different subpopulations of interneurons. In this way, the mechanisms underlying rhythms in the cortex will be uncovered; this in turn should provide further insight into the functions of cortical networks.

### Appendix: The Infinitesimal Phase Resetting Curve $Z(t)$

The intrinsic dynamics of an LIF cell are governed by the differential equation

$$\frac{dv}{dt} = -v + I,$$

which has the general solution

$$v(t) = v(t_0)e^{-(t-t_0)} + I(1 - e^{-(t-t_0)}),$$

and the condition that when  $v$  reaches a threshold of 1, it is reset to  $v = 0$ . Assuming that  $I > 1$ , the cell undergoes periodic oscillations with a period of  $T = (\ln(I/(I-1)))^{-1}$ . If the membrane potential of the cell starts out at  $v(0) = 0$ , then the evolution of  $v(t)$  for  $0 \leq t < \tilde{t} < T$  is given by

$$v(t) = I(1 - e^{-t}).$$

Suppose that a small  $\delta$ -function perturbation of strength (area)  $\varepsilon$  was delivered to the cell at a phase in the oscillation corresponding to  $t = \tilde{t}$ . This would instantaneously knock  $v$  from  $I(1 - e^{-\tilde{t}})$  to  $I(1 - e^{-\tilde{t}}) + \varepsilon$ , advancing the phase of the oscillation. To evaluate

the magnitude of the phase advance  $\Delta\phi$ , simply use  $v(\tilde{t}) = I(1 - e^{-\tilde{t}}) + \varepsilon$  as the initial condition and solve for the time that the cell reaches threshold  $v = 1$ .

$$\begin{aligned} 1 = v(T - T\Delta\phi) &= v(\tilde{t})e^{-(T-T\Delta\phi-\tilde{t})} \\ &\quad + I(1 - e^{-(T-T\Delta\phi-\tilde{t})}) \\ &= (I(1 - e^{-\tilde{t}}) + \varepsilon)e^{-(T-T\Delta\phi-\tilde{t})} \\ &\quad + I(1 - e^{-(T-T\Delta\phi-\tilde{t})}), \end{aligned}$$

which yields the firing time

$$T - T\Delta\phi = \ln \frac{I - \varepsilon e^{\tilde{t}}}{I - 1}.$$

The phase advance is

$$\begin{aligned} \Delta\phi(\tilde{t}) &= \frac{1}{T} \left( \ln \frac{I}{I-1} - \ln \frac{I - \varepsilon e^{\tilde{t}}}{I-1} \right) \\ &= \frac{1}{T} \ln \frac{I}{I - \varepsilon e^{\tilde{t}}}. \end{aligned}$$

This is the phase resetting curve for  $\delta$ -function perturbations of area  $\varepsilon$  at  $\tilde{t} < \ln(I/(I-1+\varepsilon)) < T = \ln(I/(I-1))$ . For  $\tilde{t} \geq \ln(I/(I-1+\varepsilon))$ , the perturbation immediately knocks the cell over threshold and  $v$  gets reset to 0. Therefore,  $\Delta\phi$  falls linearly from  $\ln((I-1)/(I+\varepsilon(I/(I-1+\varepsilon))))/T$  at  $\tilde{t} = \ln(I/(I-1+\varepsilon))$  to 0 at  $\tilde{t} = T$ .

Expanding  $\Delta\phi$  around the small parameter  $\varepsilon$ ,

$$\Delta\phi(\tilde{t}) = \frac{e^{\tilde{t}}}{TI} \varepsilon + O(\varepsilon^2).$$

Thus, the infinitesimal phase resetting curve (the phase dependent sensitivity function) is

$$Z(\tilde{t}) = \frac{e^{\tilde{t}}}{TI}.$$

The above derivation uses the method described in the main portion of the text, however it should be noted that there are alternative ways to obtain the phase-dependent sensitivity function  $Z(\tilde{t})$ . Up to a proportionality constant,  $Z(\tilde{t})$  can be found by solving the adjoint equation for the isolated cell linearized about the limit cycle  $v_{LC}(t)$ . The proportionality constant is chosen such that  $\langle dv_{LC}/dt, TZ \rangle_{L^2(0,T)} = 1$ . This method is usually used to calculate  $Z(\tilde{t})$  for complicated models. Also, for any single-variable integrate-and-fire model, the phase sensitivity function  $Z(\tilde{t})$  is simply  $1/(Tdv_{LC}/dt)$ .

## Acknowledgments

The authors would like to thank John Lewis and the anonymous reviewers for constructive comments on the manuscript. TJJ is supported by an National Institute of Mental Health postdoctoral fellowship MH12873.

## References

- Alvarez VA, Chow CC, VanBockstaele EJ, Williams JT (2002) Frequency-dependent synchrony in the locus ceruleus: Role of electrical coupling. *Proc. Natl. Acad. Sci. USA* 99: 4032–4036.
- Amitai Y, Gibson JR, Beierlein M, Patrick SL, Ho AM, Connors BW, Golomb D (2002) Spatial dimensions of electrically coupled networks of interneurons in neocortex. *J. Neurosci.* 22: 4142–4152.
- Beierlein M, Gibson JR, Connors BW (2000) A network of electrically coupled interneurons drives synchronized inhibition in neocortex. *Nat. Neurosci.* 3: 904–910.
- Bem T, LeFeuvre Y, Simmers J, Meyrand P (2002) Electrical coupling can prevent expression of adult-like properties in an embryonic neural circuit. *J. Neurophysiol.* 87: 538–547.
- Benardo LS (1997) Recruitment of GABAergic inhibition and synchronization of inhibitory interneurons in rat neocortex. *J. Neurophysiol.* 77: 3134–3144.
- Bressloff PC, Coombes S (1997) Synchrony in an array of integrate-and-fire neurons with dendritic structure. *Phys. Rev. Lett.* 78: 4665–4668.
- Bressloff PC, Coombes S (2000) A dynamical theory of spike train transitions in networks of integrate-and-fire oscillators. *SIAM J. Appl. Math.* 60: 820–841.
- Buhl EH, Tamas G, Fisahn A (1998) Cholinergic activation and tonic excitation induce persistent gamma oscillations in mouse somatosensory cortex in vitro. *J. Physiol. (Lond)* 513: 117–126.
- Buzsáki G, Chrobak JJ (1995) Temporal structure in spatially organized neuronal ensembles: A role for interneuronal networks. *Curr. Opin. Neurobiol.* 5: 504–510.
- Chow CC (1998) Phase-locking in weakly heterogeneous neuronal networks. *Physica D* 118: 343–370.
- Chow CC, Kopell N (2000) Dynamics of spiking neurons with electrical coupling. *Neural Comp.* 12: 1643–1678.
- Crook SM, Ermentrout GB, Bower JM (1998) Dendritic and synaptic effects in systems of coupled cortical oscillators. *J. Comput. Neurosci.* 5: 315–329.
- Erisir A, Lau D, Rudy B, Leonard S (1999) Function of specific  $K^+$  channels in sustained high-frequency firing of fast-spiking neocortical cells. *J. Neurophysiol.* 82: 2476–2489.
- Ermentrout GB (1996) Type I Membranes, phase resetting curves and synchrony. *Neural Comp.* 8: 979–1001.
- Ermentrout GB, Kleinfeld D (2001) Traveling electrical waves in cortex: Insights from phase dynamics and speculation on computational role. *Neuron* 29: 33–44.
- Ermentrout GB, Kopell N (1991) Multiple pulse interaction and averaging in coupled neural oscillators. *J. Math. Biol.* 29: 195–217.
- Ermentrout GB, Kopell N (1998) Fine structure of neural spiking and synchronization in the presence of conduction delays. *Proc. Natl. Acad. Sci. USA* 95: 1259–1264.

- Fisahn A, Pike F, Buhl EH, Paulsen O (1998) Cholinergic induction of network oscillations at 40 Hz in the hippocampus in vitro. *Nature* 394: 186–189.
- Galarreta M, Hestrin S (1999) A network of fast-spiking cells in the neocortex connected by electrical synapses. *Nature* 402: 72–75.
- Galarreta M, Hestrin S (2001a) Electrical synapses between GABA-releasing interneurons. *Nat. Rev. Neurosci.* 2: 425–433.
- Galarreta M, Hestrin S (2001b) Spike transmission and synchrony detection in networks of GABAergic interneurons. *Science* 292: 2295–2299.
- Gerstner W (1995) Time structure of the activity in neural network models. *Phys. Rev. E* 51: 738–758.
- Gibson JR, Beierlein M, Connors BW (1999) Two networks of electrically coupled inhibitory neurons in neocortex. *Nature* 402: 75–79.
- Golomb D, Hansel D, Mato G (2001) Mechanisms of synchrony of neural activity in large networks. In: F Moss, S Gielen, eds. *Handbook of Biological Physics, Vol. 4: Neuro-Informatics and Neural Modelling*. Elsevier, Amsterdam. pp. 887–968.
- Golomb D, Wang X, Rinzel J (1994) Synchronization properties of spindle oscillations in a thalamic reticular nucleus model. *J. Neurophysiol.* 72: 1109–1126.
- Grannan ER, Kleinfeld D, Sompolinsky H (1993) Stimulus dependent synchronization of neuronal assemblies. *Neural Comp.* 5: 550–569.
- Gupta A, Wang Y, Markram H (2000) Organization principles for a diversity of GABAergic interneurons and synapses in the neocortex. *Science* 287: 273–278.
- Han SK, Kurrer C, Kuramoto Y (1995) Dephasing and bursting in coupled neural oscillators. *Phys. Rev. Lett.* 75: 3190–3193.
- Hansel D, Mato G, Meunier C. (1995) Synchrony in excitatory neural networks. *Neural Comp.* 7: 307–337.
- Kopell N (1988) Toward a theory of modeling central pattern generators. In: A Cohen, ed. *Neural Control of Rhythmic Movements in Vertebrates*. John Wiley, New York. pp. 396–413.
- Kuramoto Y (1984) *Chemical Oscillations, Waves, and Turbulence*. Springer-Verlag, Berlin.
- Lewis TJ, Gibson JR, Connors BW, Rinzel J (2001) Dynamics of neurons connected by inhibitory and electrical synapses. *Society for Neuroscience Abstract* 504: 16.
- McBain CJ, Fisahn A (2001) Interneurons unbound. *Nat. Rev. Neurosci.* 2: 11–23.
- Michelson HB, Wong RK (1994) Synchronization of inhibitory neurons in the guinea-pig hippocampus in vitro. *J. Physiol. (Lond)* 92: 35–45.
- Neltner L, Hansel D, Mato G, Meunier C (2000) Synchrony in heterogeneous networks of spiking neurons. *Neural Comp.* 12: 1607–1641.
- Oviedo H, Reyes AD (2002) Boosting of neuronal firing evoked with asynchronous and synchronous inputs in the dendrite. *Nat. Neurosci.* 5: 261–266.
- Rinzel J, Ermentrout GB (1998) Analysis of neural excitability and oscillations. In: C Koch, I Segev, eds. *Methods in Neuronal Modeling: From Synapse to Networks*. MIT Press, Cambridge, MA. pp. 251–292.
- Ritz R, Sejnowski TJ (1997) Synchronous oscillatory activity in sensory systems: New vistas on mechanism. *Curr. Opin. Neurobiol.* 7: 536–546.
- Sherman A, Rinzel J (1994) Rhythmogenic effects of weak electrotonic coupling in neuronal models. *Proc. Natl. Acad. Sci. USA* 89: 2471–2474.
- Skinner FK, Zhang Y, Velazquez JLP, Carlen PL (1999) Bursting in inhibitory interneuronal networks: A role for gap-junctional coupling. *J. Neurophysiol.* 81: 1274–1283.
- Stuart G, Sakmann B (1995) Amplification of EPSPs by axosomatic sodium channels in neocortical pyramidal neurons. *Neuron* 15: 1065–1076.
- Swadlow HA, Belozerova IN, Sirota MG (1998) Sharp, local synchrony among putative feed-forward inhibitory interneurons of rabbit somatosensory cortex. *J. Neurophysiol.* 79: 567–582.
- Tamás G, Buhl EH, Lörincz A, Somogyi P (2000) Proximally targeted GABAergic synapses and gap junctions synchronize cortical interneurons. *Nat. Neurosci.* 3: 366–371.
- Traub RD (1995) Model of synchronized population bursts in electrically coupled interneurons containing active dendrites. *J. Comput. Neurosci.* 2: 283–289.
- Traub RD, Kopell N, Bibbig A, Buhl EH, LeBeau FEN, Whittington MA (2001) Gap junctions between interneuron dendrites can enhance synchrony of gamma oscillations in distributed networks. *J. Neurosci.* 21: 9478–9488.
- Usher M, Cohen JD, Servan-Schreiber D, Rajkowski J, Aston-Jones G (1999) The role of Locus Coeruleus in the regulation of cognitive performance. *Science* 283: 549–554.
- van Vreeswijk C, Abbott LF, Ermentrout GB (1994) When inhibition not excitation synchronizes neural firing. *J. Comput. Neurosci.* 1: 313–321.
- Various (1999) Reviews on the binding problem. *Neuron* 24: 7–125.
- Wang X, Buzsáki G (1996) Gamma oscillations by synaptic inhibition in an interneuronal network model. *J. Neurosci.* 16: 6402–6413.
- Wang X, Rinzel J (1992) Alternating and synchronous rhythms in reciprocally inhibitory model neurons. *Neural Comp.* 4: 84–97.
- White JA, Chow CC, Ritt J, Soto-Trevino C, Kopell N (1998) Synchronization and oscillatory dynamics in heterogeneous, mutually inhibitory neurons. *J. Comput. Neurosci.* 5: 5–16.
- Whittington MA, Standford IM, Traub RD, Jefferys JG (1997) Spatiotemporal patterns of gamma frequency oscillations tetanically induced in the rat hippocampal slice. *J. Physiol. (Lond)* 502: 591–602.
- Whittington MA, Traub RD, Jefferys JG (1995) Synchronized oscillations in interneuron networks driven by metabotropic glutamate receptor activation. *Nature* 373: 612–615.
- Ylinen A, Bragin A, Nádasdy Z, Jandó G, Szabó I, Sik A, Buzsáki G (1995) Sharp wave-associated high-frequency oscillations (200 Hz) in the intact hippocampus: Network and intracellular mechanisms. *J. Neurosci.* 15: 30–46.